Title

- A soft matter computer for soft robots

Authors

M. Garrad,[1,3,4,†] G. Soter,[1,3,†] A. T. Conn[2,3] , H. Hauser[1,3] and J. Rossiter[1*,3]

Affiliations

[1]Department of Engineering Mathematics, University of Bristol, UK.

[2]Department of Mechanical Engineering, University of Bristol, UK.

[3]SoftLab, Bristol Robotics Laboratory, UK.

[4]FARSCOPE Centre for Doctoral Training, Bristol Robotics Laboratory, UK.

[†]These authors contributed equally to this work.

[*]Correspondence to: jonathan.rossiter@bristol.ac.uk.

Abstract

Despite the growing interest in soft robotics, little attention has been paid to the development of soft matter computational mechanisms. Embedding computation directly into soft materials is not only necessary for the next generation of fully soft robots, but also for smart materials to move beyond stimulus-response relationships and towards the intelligent behaviours seen in biological systems. This article describes the Soft Matter Computer (SMC), a low-cost and easily fabricated computational mechanism for soft robots. The building block of an SMC is a conductive fluid receptor (CFR), which maps a fluidic input signal to an electrical output signal via electrodes embedded into a soft tube. SMCs can perform both analogue and digital computation. The potential of the SMC is demonstrated by integrating them into three soft robots: (i), a Softworm robot is controlled by an SMC which generates the control signals necessary for three distinct gaits; (ii), a soft gripper is given a set of reflexes which can be programmed by adjusting the parameters of the CFR; and (iii), a two degree of freedom bending actuator is switched between three distinct behaviours by varying only one input parameter. The Soft Matter Computer is a low-cost way to integrate computation directly into soft materials, and an important step towards entirely soft autonomous robots.

Summary

Conductive Fluid receptors can be used to create soft matter computers which are suitable for the control of soft robots.

MAIN TEXT

Introduction

The next generation of robotic systems must be capable of safely operating in complex, dynamic environments. Integrating soft matter into the system is an elegant way of achieving this; by exploiting the inherent compliance of soft materials, robots which adapt to—rather than resist—the environment can be developed (34, 35, 38). This insight has driven recent interest in soft robotics, leading to the development of soft matter actuation (10, 23, 59, 64), sensing (20, 27, 51, 79), and power (14, 53, 91) systems. However, far less attention has been paid to the development of soft matter mechanisms for computation. The range and complexity of behaviours that can be created using only materials-based control approaches is limited, and as a result, soft robotic systems have until now mostly been controlled by electronic microcontrollers. A better approach for soft matter systems could be to build a soft matter computational system directly into the body of the robot. This would lead to a new generation of soft robots, with levels of autonomy similar to their rigid cousins, but without sacrificing the benefits associated with soft materials.

In this paper, we introduce the conductive fluid receptor (CFR) and show it is a fundamental building block for a range of Soft Matter Computers (SMCs). The SMC concept takes inspiration from the way in which the vascular system is used in biological systems to encode and transmit information that is processed locally in distinct organs. For example, hormones such as adrenaline, are released into the bloodstream and disperse throughout the body. When detected by an appropriate receptor, hormones trigger a local response (e.g. increased blood-flow in flight muscles, and dilation of the pupils in the eyes). In a similar way, an SMC encodes information in the spatial structure of a fluidic tape which travels through the soft body. When this information is detected by an appropriate receptor, it generates an output. We show SMC architectures for performing both analogue and digital computation and a number of ways in which these simple architectures can be composed to compute more complex functions. We further demonstrate that the outputs generated by an SMC can be connected directly to soft actuators and embedded within the body of a robot, creating a range of robots with integrated soft matter controllers.

In order to introduce a new computational mechanism, we must first consider what it means to do computation in this context. We follow the widely accepted definition from (28) which defines a computer to be a physical device that can be used to perform a mapping between objects in abstract (information) space (13, 29, 42). The introduction of a new computational mechanism therefore requires that we specify an input encoding, a physical mapping and output decoding. The specific mapping performed by the computer is referred to as the program and may be fixed by the structure of the hardware or adjusted by a separate programming mechanism.

In our Soft Matter Computer, patterns of conducting and insulating fluids encode the input. As the fluid progresses, the information in the spatial pattern of the input is mapped to an electrical current by the CFRs. This output current can be used to control a variety of soft materials, actuators or even complete robots. The mapping (i.e. the program) from input to output is controlled by the length, offset and spacing of the CFR’s electrodes, allowing the designer to program a wide range of input-output mappings. These structures operate at low voltages and pressures, do not require complex fabrication processes, and can be easily interfaced with soft mechanoreceptors.

In contrast to the plethora of computational mechanisms used by biological systems (52, 54, 78), computation in synthetic devices is almost entirely performed by electronic processors. Whilst there has been significant research into unconventional mechanisms for computation (2, 18, 69), much of this work has been concerned with proving these alternatives are Turing complete (1, 41). Where practical demonstrations of such approaches have been developed, they often require the use of conventional electronic computers (71), complex mechanisms for encoding a specific input (43) or cannot be easily (re)-programmed (32).

Without practical means of integrating computation into smart materials, research has mostly been limited to engineering stimuli-response relationships (3, 16, 19). Constructing higher level behaviours, such as decision-making, adaptation, and learning, from purely reactive mechanisms is notoriously difficult (4, 46). As such, smart materials have yet to demonstrate the diversity of behaviours seen in biological materials (17, 36, 57). As a further consequence, the majority of soft robots still use control approaches developed for rigid systems (11, 39, 70), introducing rigid elements (or tethers) into otherwise soft systems, and therefore limiting their adaptability. The development of soft matter computing will enable roboticists to create a new class of entirely soft robots. In turn, these smart material-based robots will enable new possibilities in environmental monitoring, pollution clean-up, energy-harvesting, drug-delivery, wearable bio-sensing and prosthetic devices, and self-healing composites.

As a result, there is considerable interest in developing soft matter structures capable of providing the computation necessary for control of soft robots. For example, the microfluidics community has demonstrated analogues of many electronic components, including digital logic gates (9, 56, 68), and composed these to form integrated fluidic processing units (88). These devices can be fabricated using elastomeric material, composed into control systems and integrated into soft robots (58, 80, 89). However, it is not easy to interface microfluidic controllers with non-fluidic soft actuators, and even fluidic actuation is limited by the low flow rates characteristic of microfluidic systems. Alongside being directly used to control a soft robot, SMCs can complement these approaches, by interfacing microfluidic control circuits with non-fluidic soft actuators.

The SMC uses conductive fluid to transduce a fluidic signal into an electrical output. The use of conductive fluids in microfluidic circuits has previously been demonstrated by (81). This architecture can produce all 16 logic gates but suffers from high resistance (order 10 MΩ) and the use of direct current (DC) voltages. The SMC differs by using conduction perpendicular to the direction of fluid flow (enabling analog computation), low resistance (order 10 Ω) and AC current. Together, this makes the SMC suitable for directly powering soft actuators without the need for additional amplification or control electronics.

On a larger scale, both fluidic and mechanical switches suitable for controlling soft robotics have been developed. For example, (60) developed a soft valve capable of controlling a gripper and earthworm-like walking robot, and in (83) these were composed to form elementary electronic components, including 2-bit adders, shift-registers and edge-detectors. Fluidic controls have also been integrated into origami structures (37), while mechanical logic gates (63) can be directly 3D-printed into the body of the robot. In all cases, integrating the control structure into the body of the robot remains challenging. We demonstrate in this paper that SMCs can be integrated directly into the body of a robot with only minimal modification.

Another approach to embedding soft matter computation uses dielectric elastomer (DE) switches, logic devices and oscillator circuits (8, 47, 48). These devices have been composed to create flip-flops and used to control artificial muscles (49). However, DEs require additional electronics to generate the high voltages necessary for their operation and the use of thin sheets of elastomer mean they are often not robust.

Finally, many soft systems are designed to exploit the complex, passive dynamics of the body, often referred to as morphological computation (25). In morphological computation, the mechanical structure is designed such that the desired behaviour emerges from the interaction of the robot with its environment. This can reduce—or even eliminate—the need for external control (5, 6, 12, 26, 40, 44, 66, 90). However, while a simplification of the control problem can be identified in these examples, there is still no clear set of design principles which can be followed to exploit this effect.

Our approach is to design a fundamentally new computational mechanism using only soft materials. By developing soft computational mechanisms, we can achieve a closer integration of material and computational substrates, enabling soft robots to retain all of the benefits of soft materials and taking steps towards the intelligent, adaptive materials seen in natural systems. Figure 1A presents our concept for such a soft robotic system. While this level of integration is not yet possible, we demonstrate the fundamental components (Figure 1B-D) that could be combined with developments in energy storage (55) and soft sensing, to create such a robot. The SMC is the mechanism which enables all of these components, and we believe a significant step towards the kind of integrated, autonomous, soft robot shown in Figure 1A.

Here, we first introduce the concept behind the Soft Matter Computer, before demonstrating a range of fundamental computational functions, including switching, amplification, filtering, and digital logic. We then demonstrate the ease with which these structures can be integrated into, and used to control, soft robotic systems in three applications: (i), a Softworm robot that is controlled by an SMC that generates the control signals necessary for three distinct gaits, (ii), a soft gripper with programmable reflexes that we use to encode the sequence of actuation necessary to autonomously produce a power grip, and (iii), a 2 degree-of-freedom bending actuator that we switch between three distinct behaviours by varying only one input parameter. We believe that our Soft Matter Computer is an important step towards easy-to-fabricate, untethered and intelligent soft materials and robots.

Results

The Soft Matter Computer

The fundamental building block of the Soft Matter Computer is the conductive fluid receptor (CFR). A CFR consists of any (soft matter) tube with two electrodes placed in parallel to the direction of fluid flow, but on opposing sides of the tube (see Figure 2A for a schematic diagram). The electrodes may be completely in-line with each other; overlapping; or separated by an offset. The electrodes can be connected by introducing a conductive fluid into the region of the tube spanned by the electrodes. By injecting a pattern of insulating and conducting fluids into the tube, a binary control signal is generated. As this signal progresses through the tube, any electrical load in series with the CFR is switched.

A minimal Soft Matter Computer consists of a single CFR, a mechanism for creating and advancing the input (the pattern of conducting and insulating fluids) and an electrical load (e.g. an actuator) to indicate the output. Input patterns may be generated during operation of the system by a controller or pre-loaded into the tube and advanced when triggered. When operated in this second mode, the input may be advanced by mechanical pressure generation, a DC motor-powered pump, or by using the output of another CFR to drive a low-boiling point fluid powered soft pump. More complex Soft Matter Computers can be constructed by connecting multiple CFRs together, either fluidically (by placing multiple CFRs on a single tube); electrically (by connecting the outputs of multiple CFRs together, either in series or parallel); or electro-fluidically, by connecting the electrical output of one CFR to the fluidic input of another via a connection element (introduced later in this paper).

In computational terms, we consider the choice of electrode length, $L_{\text{electrode}}$, electrode offset, L_{offset}, and separation between consecutive CFRs, S, to be the program of a particular Soft Matter Computer. The pattern of conducting and insulating fluids represents the input to the SMC, with the output given by the current flowing through the electrical load(s).

Although independent of the choice of immiscible fluids, in this paper we use saturated saltwater (red liquid in figures) as the conductive fluid and air as the insulating fluid. When a CFR is powered with an AC electrical signal (with RMS voltage V_{AC}), this leads to an average on resistance of 10 Ω (and corresponding on current, I_{ON}) and an off resistance of over 10 MΩ. The on resistance is sufficiently low that many commonly used soft actuators can be driven at low voltages (5-15 V) via a CFR. We demonstrate this by using a CFR to control a pair of reverse-polarity LEDs (Figure S1A, Supplementary movie S8) and to switch both a shape-memory alloy (SMA) actuator (Figure S1B) and a low-boiling point fluid pouch motor (Figure S1C). These results show that the CFR is suitable for the control of a wide range of soft robotic systems (7, 21, 33, 62, 77).

Analogue computing

Next, we show that a single CFR can perform analogue style computation, by modifying a continuous quantity, the duty factor of the output signal, D_{out}. We further show that this modification of the duty factor can be used to allow only signals within a specific region of input parameter space to produce PWM outputs, with the remaining signals either fully amplified (i.e. output duty factor is 1) or fully filtered (i.e. output duty factor is 0). Within this region, input signals are modified according to the sign and magnitude of the effective electrode length, $L_{\text{eff}} = L_{\text{electrode}} - L_{\text{offset}}$.

In digital systems, pulse-width modulated (PWM) signals are commonly used to represent analog quantities such as voltage. PWM signals are described by a frequency and duty factor (which represents the fraction of the waveform which is high), with the duty factor used to represent the analog quantity. For example, if our system had a minimum voltage of 0 V and maximum voltage of 5 V, we would map 0 V to a PWM signal with duty factor 0, 2.5 V to a duty factor of 0.5, and 5 V to a duty factor of 1.

We consider PWM input signals, characterised by a wavelength, λ, and input duty factor, D_{in}, which represents the fraction of the input signal which is conductive (see Figure 2A, upper panel). Although PWM signals are typically described in terms of frequency, wavelength is the natural representation for our spatial input signals. Note that frequency domain versions of the plots in this section are also available in the Supplementary materials, Figure S4. We assume a constant flow rate for the input and begin our analysis once the tape has progressed an initial distance L_0, such that the left edge of the first conductive region is in contact with the start of the first electrode. We also introduce the defining parameter of the CFR geometry, the effective electrode length, $L_{\text{eff}} = L_{\text{electrode}} - L_{\text{offset}}$. This is the extent to which the two CFR electrodes overlap. A negative L_{eff} corresponds to the case where the distance between the two electrodes L_{offset}, is greater than the electrode length, $L_{electrode}$.

When passing through a CFR, a pulse of conductive fluid of length $L_{conductive} = \lambda D_{in}$ will cause an output pulse of length $L_{conductive} + L_{eff}$ (See Figure 2A for a pictorial representation of the mechanism, for cases where $L_{eff} = L_{electrode}$ and $L_{eff} < 0$) and output duty factor $D_{out} = D_{in} + L_{eff} / \lambda$. This means that the sign of L_{eff} can be used to determine whether the CFR acts as an amplifier (by increasing the duty factor, D_{out}, and thus power of the output), or filter (by decreasing the duty factor, D_{out}). The magnitude of L_{eff} determines the amount of amplification or filtering. We explore this further by considering two cases: fixed wavelength and fixed input duty factor.

Fixed Wavelength

Figure 2B plots the output duty factor for two fixed wavelengths (λ = 100 mm, top panel and λ = 25 mm, bottom panel) against input duty factor, for a range of values of L_{eff}. In the case of positive L_{eff}, low duty factor input signals produce PWM output signals, while inputs with duty factor above the cut-off value of $D_{cut\text{-}off} = 1 - (L_{eff} / \lambda)$ produce an output that is constantly on. If L_{eff} is negative, then the high-duty factor input signals will produce an output, but those with an input duty factor below $D_{cut\text{-}off} = L_{eff} / \lambda$ will not. Thus, if the input wavelength is fixed, by selecting L_{eff}, a designer can determine whether a CFR allows high or low duty factor signals to produce PWM outputs, and the cut-off value where this occurs. For example, if we create a CFR with L_{eff} = -15 mm and apply an input signal of λ = 100 mm, then only inputs with $D_{in} > D_{cut\text{-}off} = 0.15$ will result in a non-zero output. On the other hand, if L_{eff} = 10 mm, then only inputs with $D_{in} < D_{cut\text{-}off} = 0.9$ will produce a PWM output.

We confirmed these relationships by applying input signals of λ = 100 mm and duty factors ranging from 0.2 to 0.8 to a test CFR with L_{eff} of 3 mm, 10 mm and -15 mm. Figure 2C plots the corresponding duty factors. The relationship is shown to hold, with L_{eff} = 3 mm mapping to outputs slightly above the line of unity mapping (the response when input is mapped to output without change), while L_{eff} = 10 mm is further above this. As expected, L_{eff} = -15 mm maps to an output below the unity line. Note that while the high-pass filtering effect of the offset CFR was confirmed, at the highest duty factors the signal through the in-line CFR began to break apart (see supplementary materials Figure S5 for further information on this effect).

Fixed Duty Factor

Figure 2D plots the output duty factor for the case where the input duty factor is fixed (D_{in} = 0.1 top panel, and D_{in} = 0.5 bottom panel) and the wavelength is varied for the same values of L_{eff} used above. In both cases, large wavelength (i.e. low frequency) signals can pass with only minimal modification. For small wavelength signals, the output duty factor is modified, with the effect determined by the sign of L_{eff}. In the case of positive L_{eff}, low wavelength signals are amplified, with the cut-off wavelength given by $\lambda_{cut\text{-}off} = L_{eff} / (1 - D_{in})$, while in the case of negative L_{eff}, low wavelength signals are filtered, with the cut-off wavelength given by $\lambda_{cut\text{-}off} = L_{eff} / D_{in}$. For example, if we have a CFR with L_{eff} = 10 mm and D_{in} = 0.5, then signals with $\lambda < \lambda_{cut\text{-}off}$ = 20 mm will be fully amplified (i.e. D_{out} = 1). Figure S4 plots the same data as Figure 2D in the frequency domain.

We have shown that a Soft Matter Computer containing only a single receptor can perform analogue computation by modifying the duty factor of pulse width modulated (PWM) input signals. The specific computation performed by the system can be programmed in hardware (by varying the electrode length) or in software (by changing the wavelength or input duty factor of the signal). This shows that an SMC can be programmed to differentially filter PWM input signals, allowing only some signals to produce PWM outputs, while others are either fully amplified or fully filtered. This ability forms the basis of a simple behaviour switching system, demonstrated later in this paper.

Digital computation

Alongside analogue computation, it is also straightforward to conduct digital computation by electrically connecting multiple CFRs. By connecting two CFRs either in parallel or series and varying whether the CFRs are initially connected by conducting fluid or not, we can construct all fundamental binary operators, except for XOR. Note that XOR can be easily constructed by composing multiple SMC-gates. Figure 3A shows the schematics of five possible configurations. To confirm these gates function as expected, we fabricated each and used them to drive a shape-memory alloy actuator to visually indicate the output. Figure 3B shows the NOT gate, super-imposed on the current through the CFR, while Figure 3C demonstrates the remaining logic gates. Supplementary movies S9-12 show the AND, OR, NAND and NOR configurations respectively, driving the SMA output indicator. In all cases, the expected truth table output is demonstrated. Note that due to the serial and parallel addition of the respective resistances, an output driven by an AND gate will see an SMC resistance of approximately 20 Ω, while an output driven by an OR gate will see a resistance of 5 Ω.

In order to create more complex functions, it is necessary to compose multiple logic gates. To do this with the SMC, we developed an Electro-fluidic diode (ED) that sends the output of one CFR to the input of another. The Electro-fluidic diode is formed by sealing a conductive fabric heating element and a small amount of low-boiling point fluid inside a pouch motor (45) and then sealing this pouch motor inside a urethane vessel with a fluidic output port The Electro-fluidic diode converts electrical input energy (and information) to mechanical output energy (pressure). The ED requires approximately 100 mA to activate and is easily powered by the output of a CFR (87). We can compose two CFRs by using an ED as the electrical load connected to one CFR and attaching the fluidic output of the ED to the second. Figure 4A shows a composite Soft Matter Computer, while Figure 4B shows a schematic diagram of the Electro-fluidic diode. The composite SMC consists of a (mechanical) pressure driven switch (CFR1) and a CFR NOT gate (CFR2), joined by an Electro-fluidic diode. When the mechanical pump is activated, it advances the fluid in the CFR1, applying current to the Electro-fluidic diode. This generates an output pressure, which advances the fluid into CFR2. This in turn switches the output of CFR2 (an SMA powered indicator) off. Supplementary movie S13 shows this sequence. This behaviour is shown in Figure 4A, which shows keyframes of this sequence, and figure 4C, which shows the current through the two CFRs respectively. The use of the ED to make this connection causes an additional switching time of 5 seconds. By miniaturising the Electro-fluidic diode, we expect to greatly reduce both the switching delay and activation current.

The ability to compose multiple logical functions into a more complex structure enables the exploitation of the many logical and computational structures used in digital electronics. These structures could lead not only to reactive soft robots, but also systems which possess a form of memory (e.g. via composing multiple gates into a flip-flop structure).

Controlling robots with Soft Matter Computers

In order to demonstrate the potential of the SMC in robotics, we used Soft Matter Computers to control three soft robots.

Self-controlled Softworm robot

First, we show that an SMC controller can be integrated directly into the body of a Softworm robot, inspired by (76). Figure 5A shows top and side views of the SMC-Softworm with a closed channel for the fluidic input tape and spacing for two CFRs embedded into the structure. Softworms move by exploiting the contraction of two shape-memory alloy actuators embedded in their underside and the controllable friction of the two feet. By varying the contact angle of the feet, it is possible to switch between low and high-friction states. A crawling gait can be produced by creating a pattern of actuation which switches on one SMA, then after some time, switches on the second SMA. After further time, the first SMA is switched off and, finally, the second is switched off. Figure 5B shows the desired pattern in terms of SMC activation. Further details can be found in (74, 76).

To create this pattern of actuation in our SMC-Softworm, we placed the electrodes such that the spacing between electrodes (S_1, S_2, as shown in Figure 5B, C and D) was not equal and injected an amount of conductive fluid with $S_2 > L_{\text{conductive}} > S_1$. The closed-loop tape was advanced by a peristaltic pump mounted on top of the robot. Figure 5E shows key-frames of the top and side views of the CFR controlled Softworm during locomotion. The CFR controlled worm moves at a mean forward velocity of 0.333 mm/min (see supplementary movie S11). This is lower than the original Softworm (75) and is due to the low speed of the on-board peristaltic pump and the limitations on the speed with which a stable signal can be propagated through a CFR. This limitation is discussed in detail later in this paper. Note that the speed of the Softworm could also be increased by reducing the length of the channel the input flows through. In this case we chose the design that was easiest to manufacture.

Softworms have also been shown to be capable of both inching and wriggling behaviours (75). The control signals for these two gaits are shown in Figure 5C-D respectively. To create the inching gait, we altered the positioning of the CFRs such that the two CFRs divided the entire tube into two equal sections (i.e. $S_1 = S_2$). We also modified the input pattern to consist of two equal lengths of conductive fluid ($L_{\text{conductive},1}$, $L_{\text{conductive},2}$), separated by two equal lengths of insulating fluid (i.e. $L_{\text{conductive},1} = L_{\text{conductive},2} < S_1 = S_2$). To create the wriggling control signal, we varied the initial pattern of (input) fluid that was injected to the Softworm. By reducing the length of the conductive region such that $L_{\text{conductive}} < S_1 < S_2$, we altered the program of the system to create a control signal which causes the first SMA to turn off before the second SMA is actuated. Figures 5B-D show the current measured through each CFR against time, demonstrating that all three possible Softworm control signals can be created with the SMC.

Simple oscillatory signals are often sufficient to generate locomotion (50, 61). Typically, these are generated by a conventional microcontroller, either integrated into the system, or attached via a tether. The SMC represents a facile method by which a system for generating such signals can be integrated into the body of a soft robot. Although this instantiation of the SMC still uses a rigid component (in the form a peristaltic pump used to advance the input), eliminating the need for external control electronics represents a step towards untethered, fully soft robots.

Programmable reflexes in a soft robotic gripper

Next, we show how the digital computation performed by the SMC can be used to program the reflexes of a soft gripper. Figures 6A-B show the design of an SMC controller for three SMA actuated fingers. Each finger is connected to two CFRs in an OR gate configuration. These two CFRs are located along the same tube and attached to a mechanical (pressure) input containing conductive fluid. When pressure is applied to an input, the conductive fluid moves through the channels into the CFR regions. The applied voltage is selected such that the current through a single CFR provides enough heating to prime the actuator but is insufficient to activate the SMA. When further pressure is applied, the second CFR is connected, causing rapid actuation of the SMA finger. Figure 6C shows the total current flowing through the gripper when all three inputs are pressed simultaneously, while 6D shows the current when each input is pressed and released sequentially. By controlling the amount of fluid injected into the input chamber, we vary the distance the fluid has to travel through the channels before reaching the CFRs. In this way, we mechanically programmed a power grip action, in which two of the fingers perform an initial grasp, with the third actuating later. Figures 6E-F shows key-frames of this sequence, while supplementary movie S15 shows each finger activated in turn, followed by the simultaneous activation, causing the power grip.

There are a variety of cases where the delicate touch of a soft gripper is necessary, including sampling from coral reefs (67), picking fruit (15), and handling delicate materials (22). In most cases, these devices are controlled with conventional electronics via a tether. An SMC could be used alongside conventional electronics to provide a set of fast, locally controlled reflexes without requiring the integration of rigid components

Behaviour switching in a 2-DOF soft actuator

Finally, we show that a single SMC can produce multiple behaviours by varying only a single parameter of the input signal (the duty factor in this case). To demonstrate this, we designed a two degree of freedom bending actuator and controlled it with a single SMC, containing two CFRs (see Figure 7A). The first CFR (CFR1) had offset electrodes, with $L_{electrode}$ = 10 mm and L_{offset} = 25 mm. The second CFR (CFR2) was in-line with electrode length $L_{electrode}$ = 10 mm. Note that this meant the two CFRs had differing resistances, and to drive the system at a single voltage, we used a 120 Ω resistor, R, in series with CFR2 to ensure the current through each SMA was approximately the same. These two CFRs were separated by a distance of S = 40 mm. We applied an input signal with a wavelength of λ = 120 mm and varied only the duty factor. Key-frames from one of these sequences are shown in Figure 7B. With a duty factor of 0.1, the conductive region ($L_{conductive}$) had a length of 12 mm, enough to activate CFR2, but not CFR1. When applied to the bending actuator, this caused it to alternate between its resting position and one-sided bending. The trajectory generated by this input is shown in Figure 7C. Increasing the duty factor to 0.5 generated an input signal with $L_{conductive}$ = 60 mm. This switched CFR1 on and then off, before activating CFR2. This caused the actuator to switch between the two opposite bending states, via the resting state. This trajectory is shown in Figure 7D. Finally, we applied a signal with a duty factor of 0.8. This caused the CFR2 to activate before CFR1 switched off. When applied to the actuator, this generated a two-dimensional cyclic path for the end of the actuator, as shown in Figure 7E. During this sequence, the tip moved via a compressed state caused by the simultaneous activation of both SMAs. These cycles can be seen in supplementary movie S16.

By simply changing the fluid input control sequence, we were able to selectively transition between a range of actuation trajectories. Specifically, we use a change in a continuous quantity, the length $L_{\text{conductive}}$ of the conductive region, and therefore the duty factor D_{in} to switch between distinct behaviours. Using change in a continuous quantity to switch between qualitatively different behaviours has been proposed to explain the switch between swimming and walking in salamanders (31) and a range of other behaviours (24). These results suggest that an SMC can not only generate oscillatory or reflexive signals but can also be used to control robots where switching between behaviours is needed.

Discussion

This paper presents the Soft Matter Computer (SMC), a soft-matter computational mechanism that can be easily integrated into soft robots. An SMC consists of one or more Conductive Fluid Receptors (CFRs), representing the program of the SMC, and a pattern of conducting and insulating fluids as input. We have shown that even a single CFR is sufficient for performing analogue computations and that digital computation is possible with two or more CFRs. We have also shown that it is possible to compose SMCs in a variety of ways, meaning the space of possible SMC architectures is far larger than those presented in this paper.

A natural question to consider when introducing a new computational mechanism is the range of mappings it can perform. It has been shown that the composition of electronic logic gates can compute any function from the wide class of general recursive functions (72). The SMC can implement the same binary operations performed by these gates, meaning that theoretically it can be a basis for a Turing complete computational mechanism. While there are still fabrication challenges to be overcome before large-scale integrated SMC structures are feasible, there are many use cases where the minimal computation demonstrated here is sufficient. We believe the SMC is particularly suited for providing local, reflexive control for soft grippers and for generating oscillatory control signals for locomotion, without the need for conventional electronics.

Furthermore, for certain computations, we expect that an SMC architecture is a more natural fit than a traditional electronic microcontroller. The CFR represents a fundamentally different mechanism to that used by digital logic gates, with the ability to easily mix analogue and digital style computations, and with a natural representation of a pulse of information. For example, while we can simulate spiking neural networks using conventional electronics, this requires the integration of the differential equations describing the dynamics of the neuron. The SMC, on the other hand, could naturally represent the notion of a spike with a short length of conductive fluid.

We have also shown that it is possible to integrate the SMC directly into the body of a number of soft robots. This requires only the addition of a channel for the tape to flow through, the attachment of the electrodes, a suitable mechanism for advancing the tape and an AC signal source; all of which can be easily placed on-board of the system. In all three demonstrations, we have used a shape-memory alloy actuator as the output of the SMC. However, it is possible to use the output of an SMC to control any electrically or thermally driven actuator, making them suitable for controlling a wide range of robots. Furthermore, as the SMC transduces a fluidic input into an electrical output it is also capable of interfacing more technologically mature microfluidic control circuits with non-fluidic soft actuators. This vastly increases the design space for such systems, and enables the use of fast, and / or high-power soft actuators such as shape memory alloys, ionic-polymer metal composites, and pouch motors.

For an SMC-controlled robot to operate completely untethered and not require any rigid components, it is necessary to develop soft mechanisms for creating an input, advancing the input and generating an AC signal. In the simplest case, input patterns can be generated prior to operation, stored in a section of tube, and only advanced during operation (equivalent to programming a micro-controller with an external programmer). Digital SMC architectures can be used to switch between multiple pre-loaded tapes in order to create more complex behaviours. An entirely soft tape generation mechanism could be created by composing multiple SMCs into a flip-flop structure and using this to control two Electro-fluidic diode-based pumps. These ED based pumps would require the addition of an extra outlet and a check valve on each outlet to function correctly. For advancing the tape, we have demonstrated two soft mechanisms: a mechanical bellow, and the Electro-fluidic diode (ED). However, there are many alternative soft pressure sources (84-86), such as the catalysed decomposition of hydrogen peroxide, also suitable for autonomously advancing the input. On the other hand, generating an AC signal without rigid components is challenging and we are currently investigating a range of alternative conductive fluids, such as liquid metals, to eliminate the need for an AC signal.

We are also considering alternative computational mechanisms inspired by the way information is encoded in the Soft Matter Computer. In the SMC, electrodes create a response when they are bridged by a conductive fluid; the mutual conductivity of the electrodes and fluid transduces the information in the fluidic input into an electrical response. However, this principle of encoding information in the spatial structure of a fluid is independent of any specific transduction mechanism. For example, we could replace the electrodes with catalysts (e.g. Platinum), triggering a response when the correct mixture of reactants (e.g. H_2O_2) flow into the active (catalysed) region.

Throughout the development of these devices, we encountered two main limitations. Firstly, even at high frequencies, a single Conductive Fluid Receptor has a resistance of approximately 10 Ω, limiting the amount of current we can deliver. Combining units in series compounds this problem, as does adding an offset to the electrodes. Although this can be overcome by the construction of an electronic buffer circuit, this comes at the expense of added complexity. We expect that alternative conductive fluids such as liquid metals will overcome this limitation. Secondly, determinism in the SMC requires that the lengths of the conductive and non-conductive fluid regions remain approximately constant throughout operation. We tested the long-term stability of the SMC pattern, finding that at low speeds, the pattern is stable, with mean duty factor changing from 0.174 to 0.151 after 8 hours of operation (See Figure S6). We suspect that much of this variation may be due to imperfect sealing of the tube, however. However, we found that the pattern can be affected if the fluid is advanced too fast. This is due to a viscous boundary layer which forms between the saltwater and tube. At low flow rates, this viscous layer remains attached to the rest of the fluid and progresses with it. At higher speeds, this layer detaches from the fluid, to be then collected by the next section of saltwater. Finally, at high enough speeds, the depth of the viscous boundary layer is enough to connect two conductive regions. At this point, fluid does not flow along the tube in discrete elements anymore (see Figure S5 for images of the salt-water tape breaking down). Supplementary movie S17 demonstrates an SMC actuating a SMA actuator at the maximum currently attainable speed. We also found that the use of AC current means no observable electrolysis occurs during operation (See Figure S7 for a comparison of the observable electrolysis for AC and DC voltages).

Conversely, we found that the tape remained intact during body deformation. This is best observed in the SMC-Softworm, where large deformations of the body are necessary for locomotion, yet the tape remained intact throughout. We repeated the long-term stability test with a deformed tube and found that the mean duty factor reduced from 0.23 to 0.175 after 8 hours of operation (See Figure S6B). We expect that extreme deformations (enough to cause buckling within the tube), or deformation that is localized to the CFR region would, however, effect the operation of the SMC.

The interplay between the various forces affecting the tape as it progresses through the SMC also determines the length scales where the SMC concept could be applicable. The Reynolds number for flow in a tube scales linearly with the mean velocity of the fluid and the hydraulic diameter of the tube, meaning that as the SMC is miniaturized, higher fluid velocities become possible without inertial effects influencing the flow. Similarly, the balance of viscous forces to interfacial tension is captured by the dimensionless capillary number, Ca, which is linearly proportional to fluid velocity. This suggests that the SMC concept should be applicable at the micro-scale, and we are current exploring microfluidic fabrication techniques to realise this.

This paper has presented the Soft Matter Computer, a soft matter computational mechanism that can be easily integrated into soft robots and used to control a wide range of soft robots. The mechanism uses the placement of electrodes to control the way in which an input pattern of conducting and insulating fluids is mapped to an output current flowing through the electrodes. The mechanism can be used to create analogue, digital or hybrid computations, and can be easily integrated into smart materials or soft matter robots, paving the way for more sophisticated soft robots and intelligent compliant structures.

Materials and Methods

Fabrication of a Conductive Fluid Receptor (CFR)

CFRs were made from Polydimethylsiloxane (PDMS, Farnell, UK). Molds for the two halves of a CFR were first printed on an Objet Connex in Verowhite. PDMS parts A and B were mixed in a 10:1 ratio, poured into the mold and cured for 24 hours at 40º C. Once cured, gold plated copper wire electrodes were cut to length, bent to shape by hand and inserted into the CFR halves. The two halves were then sealed together with a layer of uncured PDMS and silicone tubing sealed into both ends, also with a layer of uncured PDMS. We were also able to fabricate working CFRs by hand sewing electrodes into pre-fabricated silicone tubes.

Frequency response and resistance measurements

The frequency response of a CFR was measured with a potential divider setup. A potentiostat (Hokutu Denki HA-151B) was used to provide the input voltages, with resistance calculated by measuring the voltage drop across a 10 Ω load resistor (RS Components, UK) with a data acquisition unit (NI-USB 6229, National Instruments, UK). A similar approach was used to measure the resistance when investigating the relationship between electrode offset and resistance. This setup was also used for the reliability tests. In this case, the input was advanced by the same peristaltic pump used to power the Softworm robot. The pump was operated continuously for 8 hours, with current measurements taken for 10 minutes at hourly intervals. A python script was used to calculate the duty cycle throughout this period.

Fabrication of pouch motors

Pouch motors were fabricated from polyethylene. 40 mm lengths of polyethylene tube were cut and heat sealed along one edge. Wires were hand sewn into a conductive fabric (Adafruit Knit Jersey Conductive Fabric, Farnell, UK) which formed a heating element, and this was placed into the half-sealed polyethylene. 1 ml of low boiling point fluid (Novec 7100, Sigma Aldrich, UK) was injected into the bag. Finally, the top of the bag was also heat sealed.

Fabrication of Electro-fluidic diode (ED)

The Electro-fluidic diode was made from Vytaflex 30 (Bentley Advanced Materials, UK). Molds were printed on the Objet Connex out of Tangoblack. Vytaflex parts A and B were mixed in a 1:1 ratio, degassed, poured into the mold and left to cure for 4 hours at 40º C. Separately, a lid for the chamber was cast. The pouch motor was placed inside the chamber and the connecting membrane was then sealed on top of the chamber with uncured Vytaflex 30. Once cured, an outlet hole was cut and a silicone tube sealed with further Vytaflex 30.

Fabrication of the Softworm robot

Molds for the top and bottom parts of the Softworm were printed on an Objet Connex out of Verowhite. Separately, the low friction feet of the worm were also printed in Verowhite. The Softworm was cast out of Sorta-Clear 12 (Bentley Advanced Materials, UK). Parts A and B were mixed in a 1:1 ratio, degassed and poured into the mold. After curing for 4 hours at 40º C, gold-plated copper electrodes were cut, shaped by hand and placed into the appropriate locations. The two halves were then sealed together with a layer of uncured elastomer. The two feet were also attached with a layer of uncured elastomer. Finally, SMA actuators were cut to length and threaded through the body of the Softworm. Two short lengths of silicone tubing were attached to each end of the fluid channel and attached to a micro peristaltic pump (RP-Q1 Miniature peristaltic pump, Takasago Electric).

Fabrication of the gripper

Molds for the gripper base were printed in Verowhite on an Objet Connex. PDMS elastomer was mixed in a 10:1 ratio, poured into the molds and allowed to cure for 24 hours at 40º C. Once cured, electrodes were cut to length, bent to shape and placed in by hand. The two halves were then sealed together with a further layer of uncured elastomer. Separately, a two-part mold for the input domes was printed on the Objet Connex (top part Verowhite, lower part Tangoblack). PDMS was mixed as before and poured into the lower mold. The upper mold was then pressed into the lower mold. Once cured, the domes were sealed on top of the gripper with a further layer of uncured PDMS. Three fingers were printed on an Objet Connex in Tangoblack. SMA actuators were threaded into the channels shown in

Figure 6. The fingers were bonded into the gripper using Sil-Poxy. Finally, a mixture of salt, water and red food dye was mixed and injected into the input chambers.

References and Notes

1. A. Adamatzky, Collision-based computing in Belousov–Zhabotinsky medium, *Chaos, Solitons & Fractals* **21**, 1259–1264 (2004).

2. A. Adamatzky, From utopian to genuine unconventional computers, *Luniver Press*, (2006).

3. E. Borré, J. F. Stumbé, S. Bellemin-Laponnaz, M. Mauro, Light-powered self-healable metallosupramolecular soft actuators, *Angewandte Chemie* **128**, 1335–1339 (2016).

4. V. Braitenberg, Vehicles: Experiments in synthetic psychology, *IT press*, (1986).

5. E. Brown, N. Rodenberg, J. Amend, A. Mozeika, E. Steltz, M. R. Zakin, H. Lipson, H. M Jaeger, Universal robotic gripper based on the jamming of granular material, *Proceedings of the National Academy of Sciences* **107,** 18809–18814 (2010).

6. M. Calisti, Soft robotics in underwater legged locomotion: From octopus–inspired solutions to running robots, *Soft Robotics: Trends, Applications and Challenges*, 31–36 (2017).

7. S. Y. Chang, K. Takashima, S. Nishikawa, R. Niiyama, T. Someya, H. Onodera, Y. Kuniyoshi, Design of small-size pouch motors for rat gait rehabilitation device, *37^{th} Annual International Conference of the IEEE Engineering in Medicine and Biology Society*, 4578-4581 (2015).

8. N. Chau, G. A. Slipher, B. M. O'Brien, R. A. Mrozek, I. A. Anderson, A solid-state dielectric elastomer switch for soft logic, *Applied Physics Letters* **108,** 103506 (2016).

9. L. F. Cheow, L. Yobas, D. L. Kwong, Digital microfluidics: Droplet based logic gates, *Applied Physics Letters* **90,** 054107 (2007).

10. M. Cianchetti, Fundamentals on the use of shape memory alloys in soft robotics, *Interdisciplinary Mechatronics: Engineering Science and Research Development*, 227–254 (2013).

11. M. Cianchetti, T. Ranzani, G. Gerboni, T. Nanayakkara, K. Althoefer, P. Dasgupta, A. Menciassi, Soft robotics technologies to address shortcomings in today's minimally invasive surgery: the stiff-flop approach, *Soft Robotics* **1,** 122–131 (2014).

12. S. Collins, A. Ruina, R. Tedrake, M. Wisse, Efficient bipedal robots based on passive-dynamic walkers. *Science* **307**, 1082–1085 (2005).

13. G. Dodig-Crnkovic, The info-computational nature of morphological computing, *Philosophy and Theory of Artificial Intelligence*, 59–68 (2013).

14. M. Duranti, M. Righi, R. Vertechy, M. Fontana, A new class of variable capacitance generators based on the dielectric fluid transducer, *Smart Materials and Structures* **26**, 115014 (2017).

15. K. Elgeneidy, P. Liu, S. Pearson, N. Lohse, G. Neumann, Printable soft grippers with integrated bend sensing for handling of crops, *Towards Autonomous Robotic Systems: 19th Annual Conference* **10965**, 479-480 (2018).

16. B. Florijn, C. Coulais, M. van Hecke, Programmable mechanical metamaterials, *Physical Review Letters* **113,** 175503 (2014).

17. P. Fratzl, F. G. Barth, Biomaterial systems for mechanosensing and actuation, *Nature* **462,** 442-448 (2009).

18. E. Fredkin, T. Toffoli, Conservative logic, *International Journal of Theoretical Physics* **21**, 219–253 (1982).

19. R. Gatt, L. Mizzi, J. I. Azzopardi, K. M. Azzopardi, D. Attard, A. Casha, J. Briffa, J. N. Grima, Hierarchical auxetic mechanical metamaterials, *Scientific Reports* **5**, 8395 (2015).

20. T. A. Gisby, B. M. O'Brien, I. A. Anderson, Self-sensing feedback for dielectric elastomer actuators, *Applied Physics Letters* **102**, 193703 (2013).

21. J. D. Greer, T. K. Morimoto, A. M. Okamura, E. W. Hawkes, Series pneumatic artificial muscles (spams) and application to a soft continuum robot, *IEEE International Conference on Robotics and Automation*, 5503–5510 (2017).

22. J. Guo, K. Elgeneidy, C. Xiang, N. Lohse, L. Justham, J. Rossiter, Soft pneumatic grippers embedded with stretchable electroadhesion, *Smart Materials and Structures* **27**, 055006 (2018).

23. C. S. Haines, M. D. Lima, N. Li, G. M. Spinks, J. Foroughi, J. D. W. Madden, S. H. Kim, S. Fang, M. J. de Andrade, F. Göktepe, Artificial muscles from fishing line and sewing thread, *Science* **343**, 868–872 (2014).

24. H. Hauser, F. Corucci, Morphosis– taking morphological computation to the next level, *Soft Robotics: Trends, Applications and Challenges*, 117–122 (2017).

25. H. Hauser, A. J. Ijspeert, R. M. Füchslin, R. Pfeifer, W. Maass, Towards a theoretical foundation for morphological computation with compliant bodies, *Biological Cybernetics* **105**, 355–370 (2011).

26. H. Hauser, A. J. Ijspeert, R. M. Füchslin, R. Pfeifer, W. Maass, The role of feedback in morphological computation with compliant bodies, *Biological Cybernetics* **106**, 595–613 (2012).

27. T. Helps, J. Rossiter, Proprioceptive flexible fluidic actuators using conductive working fluids, *Soft Robotics* **5**, 175–189 (2018).

28. C. Horsman, S. Stepney, R. C. Wagner, V. Kendon, When does a physical system compute? *Proceedings of the Royal Society A, Mathematical, Physical and Engineering Sciences* **470**, 20140182 (2014).

29. D. C. Horsman, Abstraction/representation theory for heterotic physical computing, *Philosophical Transactions of the Royal Society A* **373**, 20140224 (2015).

30. A. J. Ijspeert, Central pattern generators for locomotion control in animals and robots: a review, *Neural Networks* **21**, 642–653 (2008).

31. A. J. Ijspeert, A. Crespi, D. Ryczko, J. M. Cabelguen, From swimming to walking with a salamander robot driven by a spinal cord model, *Science* **315**, 1416–1420 (2007).

32. C. Isenberg, The soap film: An analogue computer: Soap films provide a simple method of obtaining analogue solutions to some mathematical problems, *American Scientist* **64**, 514–518 (1976).

33. B. Kim, M. G. Lee, Y. P. Lee, Y. I. Kim, G. H. Lee, An earthworm-like micro robot using shape memory alloy actuator, *Sensors and Actuators A: Physical* **125**, 429–437 (2006).

34. S. Kim, C. Laschi, B. Trimmer, Soft robotics: a bioinspired evolution in robotics, *Trends in Biotechnology* **31**, 287–294 (2013).

35. C. Laschi, B. Mazzolai, M. Cianchetti, Soft robotics: Technologies and systems pushing the boundaries of robot abilities, *Science Robotics* **1**, 3690 (2016).

36. M. Lévesque, É. Villiard, S. Roy, Skin wound healing in axolotls: a scarless process, *Journal of Experimental Zoology Part B: Molecular and Developmental Evolution* **314**, 684–697 (2010).

37. S. Li, K. W. Wang, Fluidic origami with embedded pressure dependent multi-stability: a plant inspired innovation, *Journal of The Royal Society Interface* **12**, 20150639 (2015).

38. C. Majidi, Soft robotics: a perspective-current trends and prospects for the future. *Soft Robotics* **1**, 5–11 (2014).

39. A. D. Marchese, C. D. Onal, D. Rus, Autonomous soft robotic fish capable of escape maneuvers using fluidic elastomer actuators, *Soft Robotics* **1**, 75–87 (2014).

40. T. McGeer, Passive dynamic walking, *International Journal of Robotic Research* **9**, 62–82 (1990).

41. K. Morita, Reversible computing and cellular automata - a survey, *Theoretical Computer Science* **395**, 101–131 (2008).

42. V. C. Müller, M. Hoffmann, What is morphological computation? on how the body contributes to cognition and control, *Artificial Life* **23**, 1–24 (2017).

43. T. Nakagaki, H. Yamada, Á. Tóth, Intelligence: Maze-solving by an amoeboid organism, *Nature* **407**, 470-470 (2000).

44. K. Nakajima, H. Hauser, R. Kang, E. Guglielmino, D. G. Caldwell, R. Pfeifer, A soft body as a reservoir: case studies in a dynamic model of octopus-inspired soft robotic arm, *Frontiers in Computational Neuroscience* **7**, 91 (2013).

45. R. Niiyama, X. Sun, C. Sung, B. An, D. Rus, S. Kim, Pouch motors: Printable soft actuators integrated with computational design, *Soft Robotics* **2**, 59–70 (2015).

46. S. Nolfi, Power and the limits of reactive agents, *Neurocomputing* **42**, 119–145 (2002).

47. B. M. O'Brien, I. A. Anderson, An artificial muscle computer, *Applied Physics Letters* **102**, 104102 (2013).

48. B. M. O'Brien, E. P. Calius, T. Inamura, S. Q. Xie, I. A. Anderson, Dielectric elastomer switches for smart artificial muscles, *Applied Physics A* **100**, 385–389 (2010).

49. B. M. O'Brien, T. G. McKay, S. Q. Xie, E. P. Calius, I. A. Anderson, Dielectric elastomer memory, *Electroactive Polymer Actuators and Devices* **7976**, 797621 (2011).

50. C. D. Onal, D. Rus, Autonomous undulatory serpentine locomotion utilizing body dynamics of a fluidic soft robot, *Bioinspiration & Biomimetics* **8**, 026003 (2013).

51. Y.L. Park, C. Majidi, R. Kramer, P. Bérard, R. J. Wood, Hyperelastic pressure sensing with a liquid-embedded elastomer, *Journal of Micromechanics and Microengineering* **20**, 125029 (2010).

52. G. Paun, Membrane computing: an introduction, *Springer Science & Business Media*, (2012).

53. R. Pelrine, R. Kornbluh, J. Eckerle, P. Jeuck, S. Oh, Q. Pei, S. Stanford, Dielectric elastomers: Generator mode fundamentals and applications, *Proceedings of SPIE - The International Society for Optical Engineering* **4329**, 07 (2001).

54. R. Pfeifer, G. Gómez, Morphological computation–connecting brain, body, and environment, *Creating brain-like intelligence, Lecture Notes in Computer Science* **5436**, 66–83 (2009).

55. H. Philamore, J. Rossiter, I. Ieropoulos, An energetically autonomous robotic tadpole with single membrane stomach and tail, *Conference on Biomimetic and Biohybrid Systems*, 366–378 (2015).

56. M. Prakash, N. Gershenfeld, Microfluidic bubble logic, *Science* **315**, 832–835 (2007).

57. M. D. Ramirez, T. H. Oakley, Eye-independent, light-activated chromatophore expansion (lace) and expression of phototransduction genes in the skin of octopus bimaculoides, *Journal of Experimental Biology* **218**, 1513–1520 (2015).

58. T. Ranzani, S. Russo, N. W. Bartlett, M. Wehner, R. J. Wood, Increasing the dimensionality of soft microstructures through injection-induced self-folding, *Advanced Materials* **30**, 1802739 (2018).

59. S. Rosset, H. R. Shea, Flexible and stretchable electrodes for dielectric elastomer actuators, *Applied Physics A* **110**, 281–307 (2013).

60. P. Rothemund, A. Ainla, L. Belding, D. J. Preston, S. Kurihara, Z. Suo, G. M. Whitesides, A soft, bistable valve for autonomous control of soft actuators, *Science Robotics* **3**, 7986 (2018).

61. S. Seok, C. D. Onal, R. Wood, D. Rus, S. Kim, Peristaltic locomotion with antagonistic actuators in soft robotics, *IEEE International Conference on Robotics and Automation*, 1228–1233 (2010).

62. S. Seok, C. D. Onal, K. J. Cho, R. J. Wood, D. Rus, S. Kim, Meshworm: a peristaltic soft robot with antagonistic nickel titanium coil actuators, *IEEE/ASME Transactions on mechatronics* **18**, 1485–1497 (2013).

63. Y. Song, R. M. Panas, S. Chizari, L. A. Shaw, J. A. Jackson, J. B. Hopkins, A. J. Pascall, Additively manufacturable micro-mechanical logic gates, *Nature Communications* **10**, 882 (2019).

64. K. Suzumori, S. Iikura, H. Tanaka, Flexible microactuator for miniature robots, *IEEE Micro Electro Mechanical Systems*, 204 – 209 (1991).

65. M. Taghavi, T. Helps, B. Huang, J. Rossiter, 3D-printed ready-to use variable-stiffness structures, *IEEE Robotics and Automation Letters* **3**, 2402–2407 (2018).

66. R. Tedrake, T. W. Zhang, H. S. Seung, Learning to walk in 20 minutes, *Proceedings of the Fourteenth Yale Workshop on Adaptive and Learning Systems* **95585**, 1939–1412 (2005).

67. Z. E. Teoh, B. T. Phillips, K. P. Becker, G. Whittredge, J. C. Weaver, C. Hoberman, D. F. Gruber, R. J. Wood, Rotary-actuated folding polyhedrons for midwater investigation of delicate marine organisms, *Science Robotics* **3**, 5276 (2018).

68. M. W. Toepke, V. V. Abhyankar, D. J. Beebe, Microfluidic logic gates and timers, *Lab on a Chip* **7**, 1449–1453 (2007).

69. T.Toffoli, Reversible computing, *International Colloquium on Automata, Languages, and Programming*, 632–644 (1980).

70. M. T. Tolley, R. F. Shepherd, B. Mosadegh, K. C. Galloway, M. Wehner, M. Karpelson, R. J. Wood, G. M. Whitesides, A resilient, untethered soft robot, *Soft Robotics* **1**, 213–223 (2014).

71. S. Tsuda, S. Artmann, K. P. Zauner, The phi-bot: a robot controlled by a slime mould, In *Artificial Life Models in Hardware*, 213–232 (2009).

72. A. M. Turing, On computable numbers, with an application to the entscheidungsproblem, *Proceedings of the London Mathematical Society* **2**, 230–265 (1937).

73. T. Umedachi, K. Takeda, T. Nakagaki, R. Kobayashi, A. Ishiguro, Fully decentralized control of a soft-bodied robot inspired by true slime mold, *Biological Cybernetics* **102,** 261–269 (2010).

74. T. Umedachi, B. A. Trimmer, Design of a 3D-printed soft robot with posture and steering control, *IEEE International Conference on Robotics and Automation*, 2874–2879 (2014).

75. T. Umedachi, V. Vikas, B. A. Trimmer, Highly deformable 3D printed soft robot generating inching and crawling locomotions with variable friction legs, *IEEE/RSJ International Conference on Intelligent Robots and Systems*, 4590– 4595 (2013).

76. T. Umedachi, V. Vikas, B. A. Trimmer, Softworms: the design and control of non-pneumatic, 3D-printed, deformable robots, *Bioinspiration & Biomimetics* **11**, 025001 (2016).

77. A. Villanueva, C. Smith, S. Priya, A biomimetic robotic jellyfish (robojelly) actuated by shape memory alloy composite actuators, *Bioinspiration & Biomimetics* **6**, 036004 (2011).

78. J. V. Neumann, The computer and the brain, *Yale University Press*, (2012).

79. B. Ward-Cherrier, N. Pestell, L. Cramphorn, B. Winstone, M. E. Giannaccini, J. Rossiter, N. F. Lepora, The tactip family: Soft optical tactile sensors with 3D-printed biomimetic morphologies, *Soft Robotics* **5**, 216– 227 (2018).

80. M. Wehner, R. L. Truby, D. J. Fitzgerald, B. Mosadegh, G. M. Whitesides, J. A. Lewis, R. J. Wood, An integrated design and fabrication strategy for entirely soft, autonomous robots. *Nature* **536**, 451 (2016).

81. B. Zhou, L. Wang, S. Li, X. Wang, Y.S. Hui, W. Wen, Universal logic gates via liquid-electronic hybrid divider, *Lab on a Chip* **12**, 5211-5217 (2012).

82. P. Zhu, L. Wang, Passive and active droplet generation with microfluidics: a review, *Lab on a Chip* **17**, 34–75 (2017).

83. D. J. Preston, P. Rothemund, H. J. Jiang, M. P. Nemitz, J. Rawson, Z. Suo, G. M. Whitesides, Digital logic for soft devices, *Proceedings of the National Academy of Sciences* **116**, 7750-7759 (2019).

84. C. D. Onal, X. Chen, G. M. Whitesides, D. Rus, Soft mobile robots with on-board chemical pressure generation, *Robotics Research*, 525-540 (2017).

85. M. Wehner, M. T. Tolley, Y. Mengüç, Y. L. Park, A. Mozeika, Y. Ding, C. Onal, R. F. Shepherd, G. M. Whitesides, R. J. Wood, Pneumatic energy sources for autonomous and wearable soft robotics, *Soft Robotics* **1**, 263-274 (2014).

86. C. Cao, X. Gao, A.T. Conn, A Magnetically Coupled Dielectric Elastomer Pump for Soft Robotics, *Advanced Materials Technologies*, 1900128 (2019).

87. M. Garrad, G. Soter, A. T. Conn, H. Hauser, J. Rossiter, Driving Soft Robots with Low-Boiling Point Fluids, *IEEE Conference on Soft Robotics*, 74-79 (2019).

88. T. Thorsen, S. J. Maerkl, S. R. Quake, Microfluidic large-scale integration, *Science* **298**, 580-584 (2002).

89. S. T. Mahon, A. Buchoux, M. E. Sayed, L. Teng, A. A Stokes, Soft Robots for Extreme Environments: Removing Electronic Control, *IEEE Conference on Soft Robotics*, 782-787 (2019)

90. M. Garrad, J. Rossiter, H. Hauser, Shaping behaviour with adaptive morphology, *IEEE Robotics and Automation Letters* **3**, 2056-2062 (2018).

91. C. A. Aubin, S. Choudhury, R. Jerch, L. A. Archer, J. H. Pikul, R. F. Shepherd, Electroylitic vascular systems for energy-dense robots, *Nature*, (2019).

Acknowledgments

Funding. This work was supported by the EPSRC Centre for Doctoral Training in Future Robotics and Autonomous Systems (FARSCOPE) EP/L015293/1. Soter is supported by the EPSRC through DTP funding. Rossiter is supported by EPSRC grants EP/M026388/1, EP/M020460/1, and EP/R02961X/1 and by the Royal Academy of Engineering as a chair in Emerging Technologies. Hauser is supported by Leverhulme Trust Project RPG-2016-345. Conn is supported by EPSRC grants EP/P025846/1 and EP/R02961X/1.

Author contributions: M.G., G.S., A.T.C, H.H. and J.R. jointly conceived of soft matter computer and all device concepts. M.G. and G.S. designed experiments, manufactured devices, collected data, performed analysis, interpreted results, wrote the manuscript and

created movies. A.T.C., H.H. and J.R. advised on all parts of the project and reviewed manuscript.

Competing interests: There are no competing interests.

Data and materials availability: Data supporting this paper is available at the University of Bristol data repository: [DOI will be provided before publication]

Figures and Tables

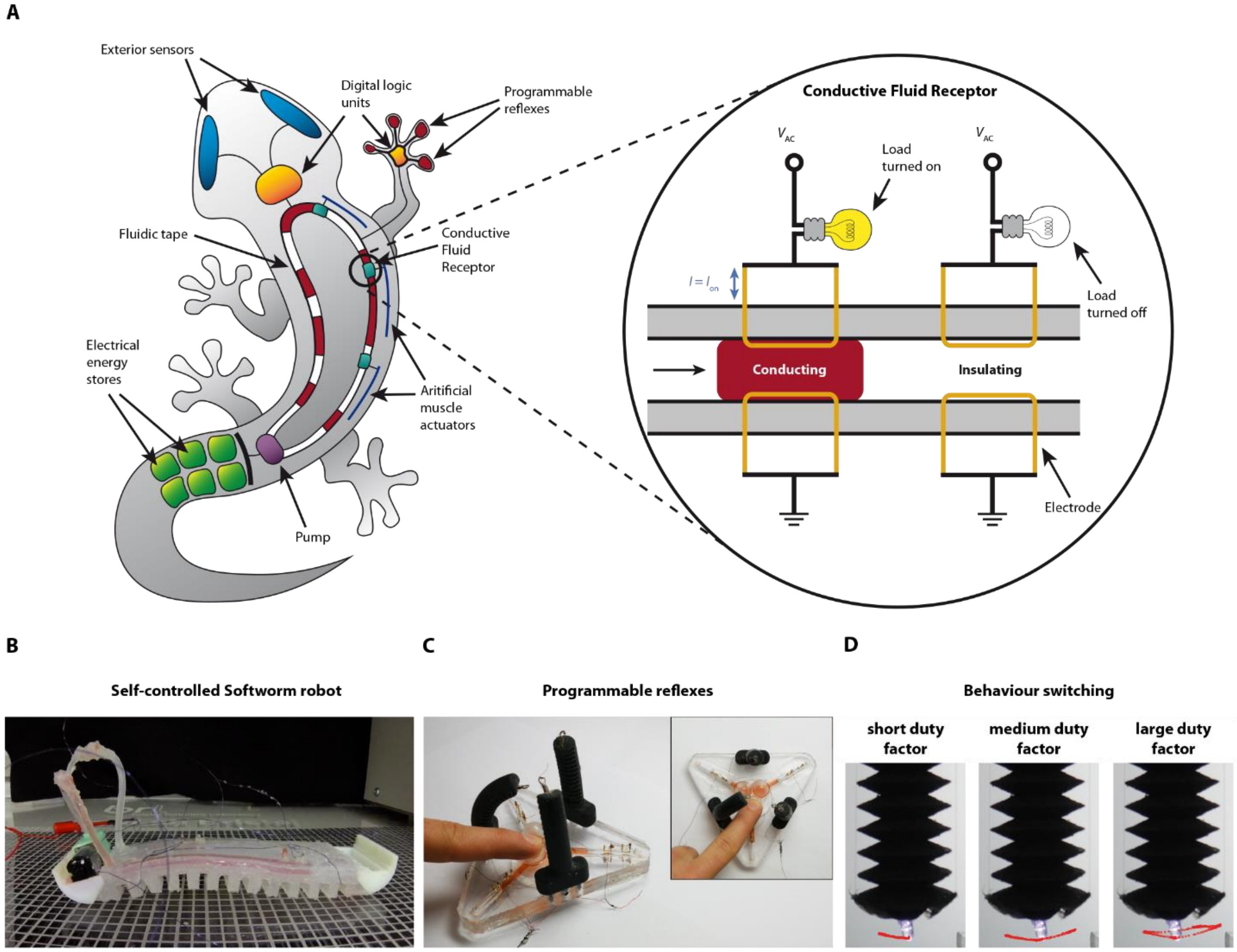

Fig. 1. The Soft Matter Computer (SMC). (A) (left) A concept for an entirely soft, entirely autonomous robot with integrated Soft Matter Computer control. This paper demonstrates a number of the individual components necessary for such a robot. The building block of the SMC is the conductive fluid receptor (right). Two electrodes are connected in series with an electrical load. When conductive fluid is injected into the region between these electrodes, the load is switched on. **(B)** An SMC controlled Softworm robot, capable of producing three behaviours. **(C)** A soft gripper with programmable reflexes provided by an integrated SMC controller. **(D)** A two-DOF bending actuator that can be switched between three behaviours (i.e. tip trajectories) by varying a single parameter of the input.

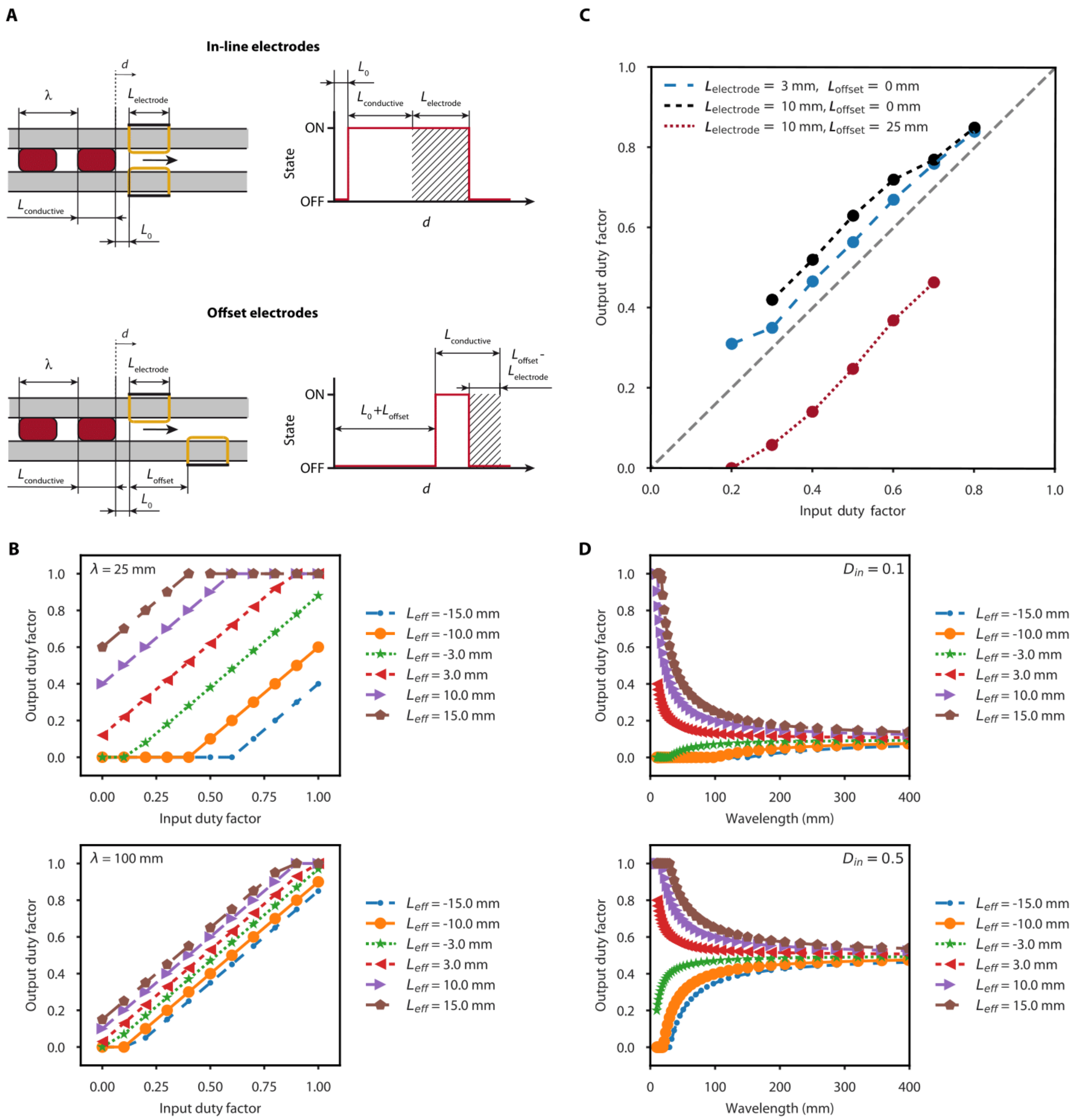

Fig. 2. Analogue soft matter computing. (A) The mechanisms by which the in-line (top) and offset (bottom) versions of the CFR can filter or amplify respectively the duty factor of PWM input signals. The right-hand images show the idealised output of each CFR, with the effect of the CFR geometry on the input signal (wavelength λ, conductive region length $L_{conductive} = \lambda D_{in}$) shown in the shaded region. **(B)** the relationship between input duty factor D_{in} and output duty factor D_{out} for fixed wavelengths of λ = 25 mm (top) and λ = 100 mm (bottom), **(C)** The output duty factor is plotted against input duty factor for three CFR geometries and an input of λ = 100 mm and duty factors D_{in} ranging from 0.2 to 0.8 and **(D)** the relationship between input wavelength λ and output duty factor D_{out} for input duty factors of D_{in} = 0.1 (top) and D_{in} = 0.5 (bottom).

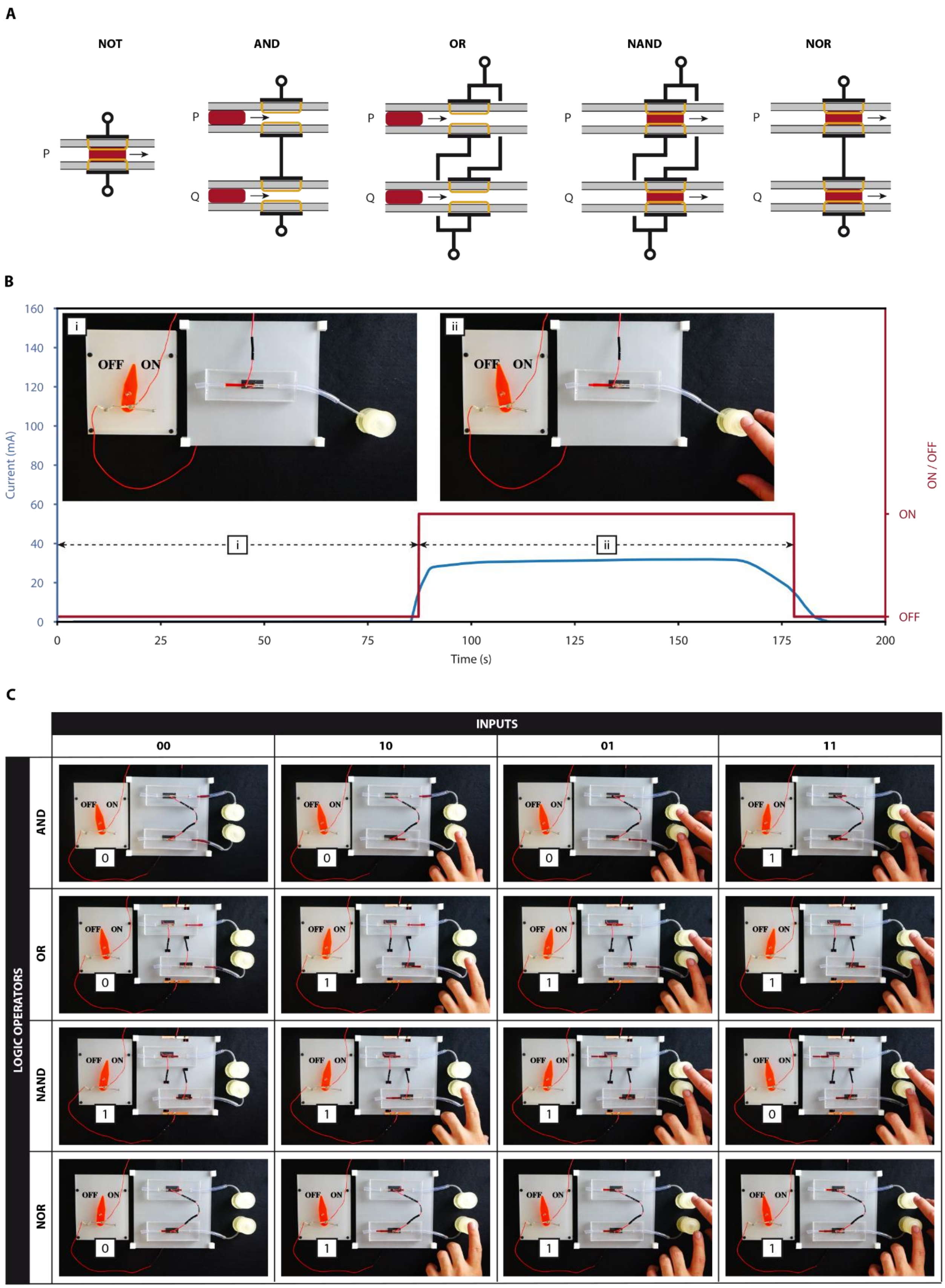

Fig. 3. CFR logic elements. (A) By connecting two CFRs either in parallel or serial, all fundamental logic elements bar XOR can be built. **(B)** A NOT gate is used to drive a shape memory alloy actuator**. (C)** The full truth tables are demonstrated for the remaining logic elements.

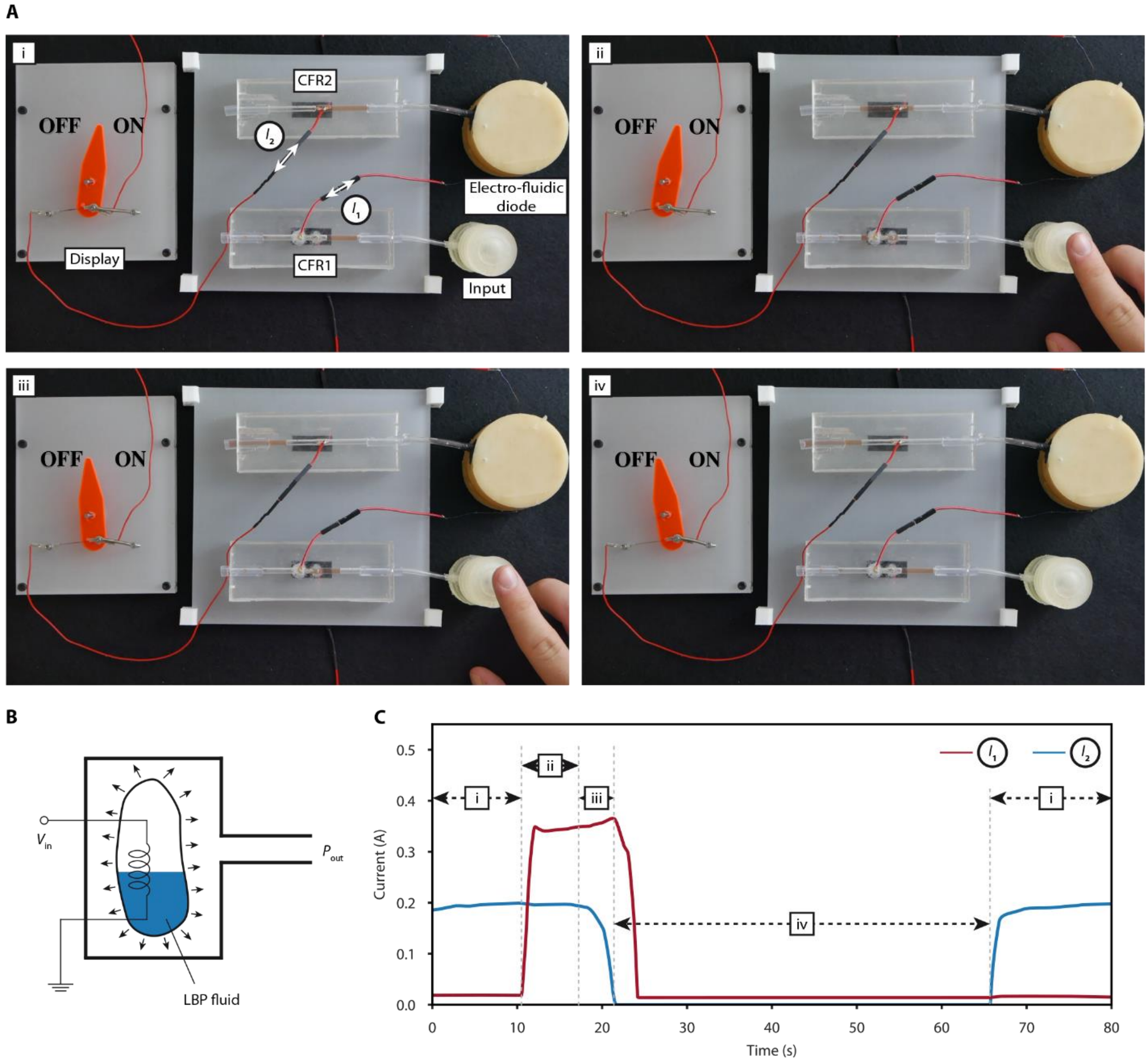

Fig. 4. Composition of digital CFRs. (A) A composite SMC, consisting of two SMCs, an Electro-fluidic diode, a mechanical pressure input and a shape memory alloy actuated display are shown. CFR1 is in the *switch* configuration, has an input advanced by a mechanical pump and has the Electro-fluidic diode as its output. CFR2 is in the NOT gate configuration, has an input advanced by the Electro-fluidic diode and has an SMA driven display as its output. In i), the mechanical pump is switched off, meaning the input to CFR1 is also off. As CFR2 is a NOT gate, this means the display is turned on. In ii), the mechanical input is turned on, connecting CFR1 and causing current to flow. This current drives the pouch motor inside the Electro-fluidic diode. In iii), the pressure generated by the Electro-fluidic diode has advanced the conductive fluid beyond CFR2, switching the display off. In iv), mechanical switch is released, switching CFR1 off. The output remains off while the fluid inside the Electro-fluidic diode returns to its initial position. **(B)** A schematic of the Electro-fluidic diode. When a voltage V_{in} is applied to the conductive fabric heating element, the resultant Joule heating causes the low boiling point (LBP) fluid to boil. This increases the pressure P_{out} at the outlet of Electro-fluidic diode. **(C)** The current through the two CFRs during this sequence.

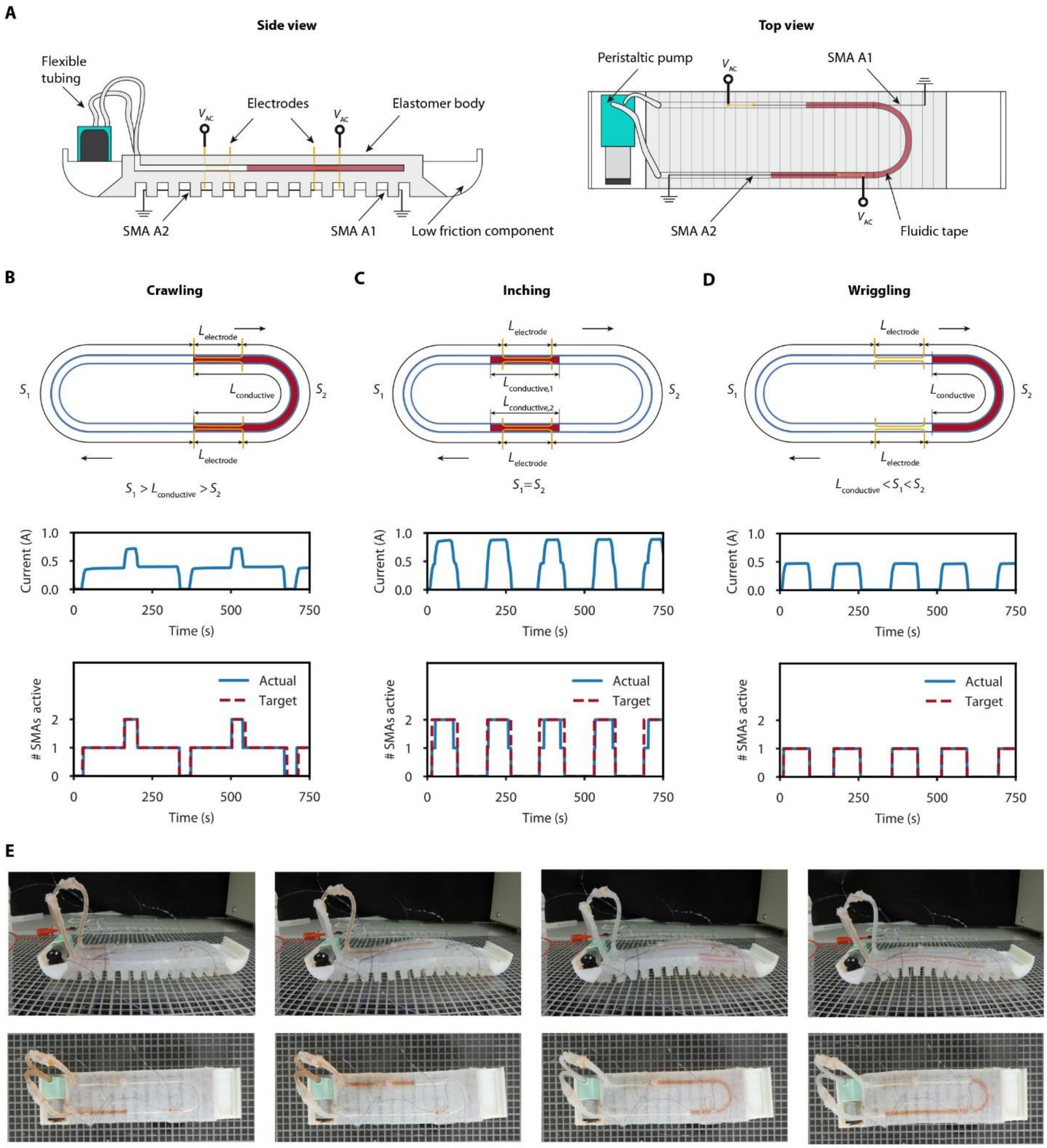

Fig. 5. A Softworm with integrated SMC controller. (A) A schematic diagram from both side and top views. **(B) - (D)** The input patterns required to produce crawling, inching and wriggling gait respectively, with the current drawn by the Softworm below. **(E)** Both top and side views of the crawling gait.

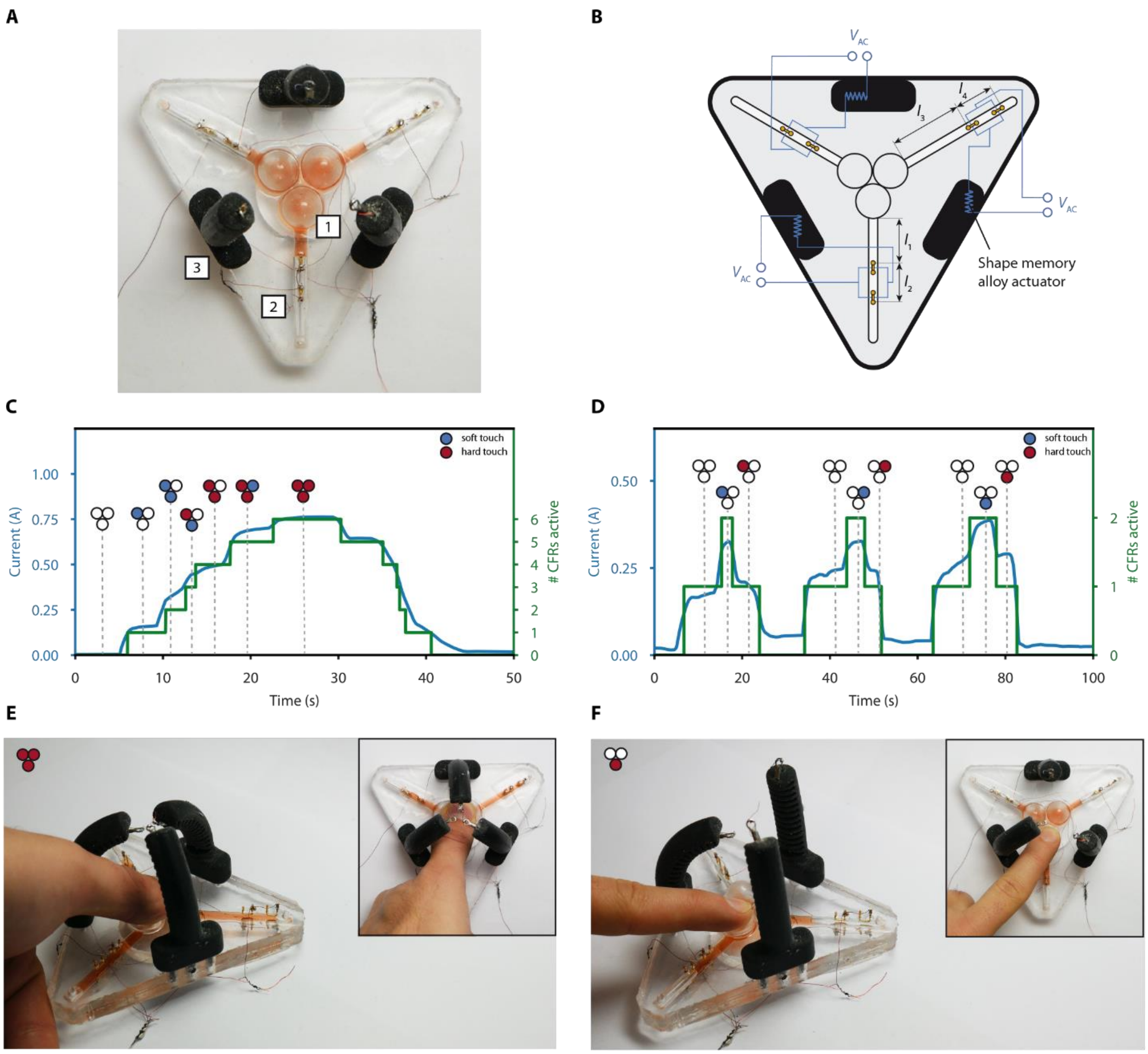

Fig. 6. Programmable reflex gripper. (A) A top view and **(B)** a schematic diagram of the gripper. **(C)** The current through the gripper during pressing of all three inputs (simultaneously). **(D)** The current through the gripper for a sequence of three individual presses, stimulating a different finger for each of the presses. **(E)** The top and side views of the fully actuated gripper. **(F)** The top and side views when the bottom pressure input is pressed and the left finger actuating in response.

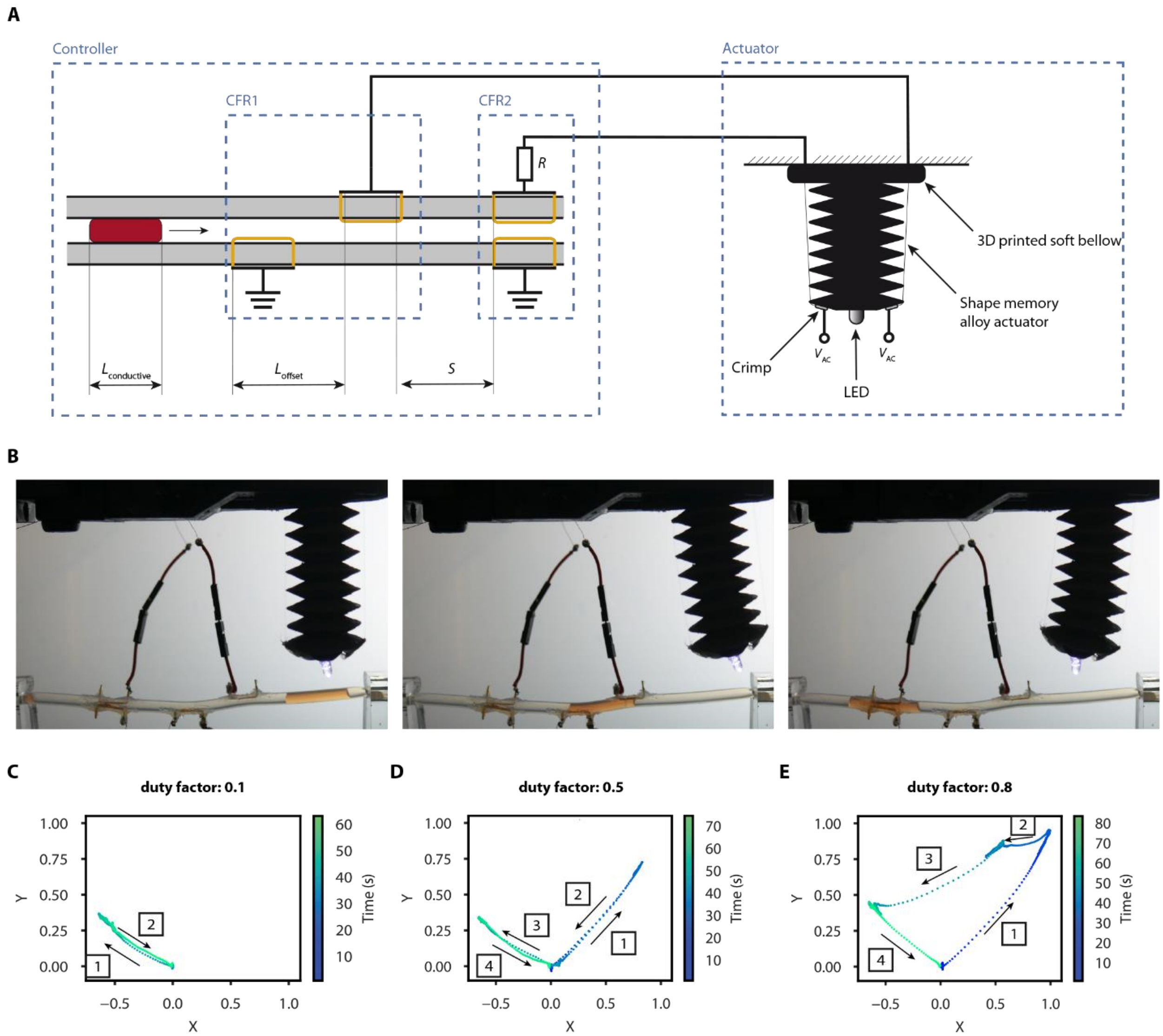

Fig. 7. Behaviour switching by varying a single input variable. (A) Schematic diagrams of both the Soft Matter Computer and two degree of freedom bending actuator. Briefly, the SMC consists of two CFRs separated by a distance S = 40 mm. Both CFRs have electrodes of length $L_{\text{electrode}}$ = 10 mm. CFR1 has an offset L_{offset} = 25 mm, while CFR2 has an offset L_{offset} = 0 mm. A resistance of $R = 120\ \Omega$ is placed in series with CFR2. **(B)** Three key-frames from the behaviour produced when driven with an input signal with a duty factor of 0.5. **(C)** Tip trajectory when the SMC is given an input with a short (0.1) duty factor. **(D)** The tip trajectory when the SMC is given an input with a medium (0.5) duty factor. **(E)** The tip trajectory when the SMC is given an input with a large (0.8) duty factor. In (C)-(E), both X and Y are normalised dimensions.

SUPPLEMENTARY MATERIALS

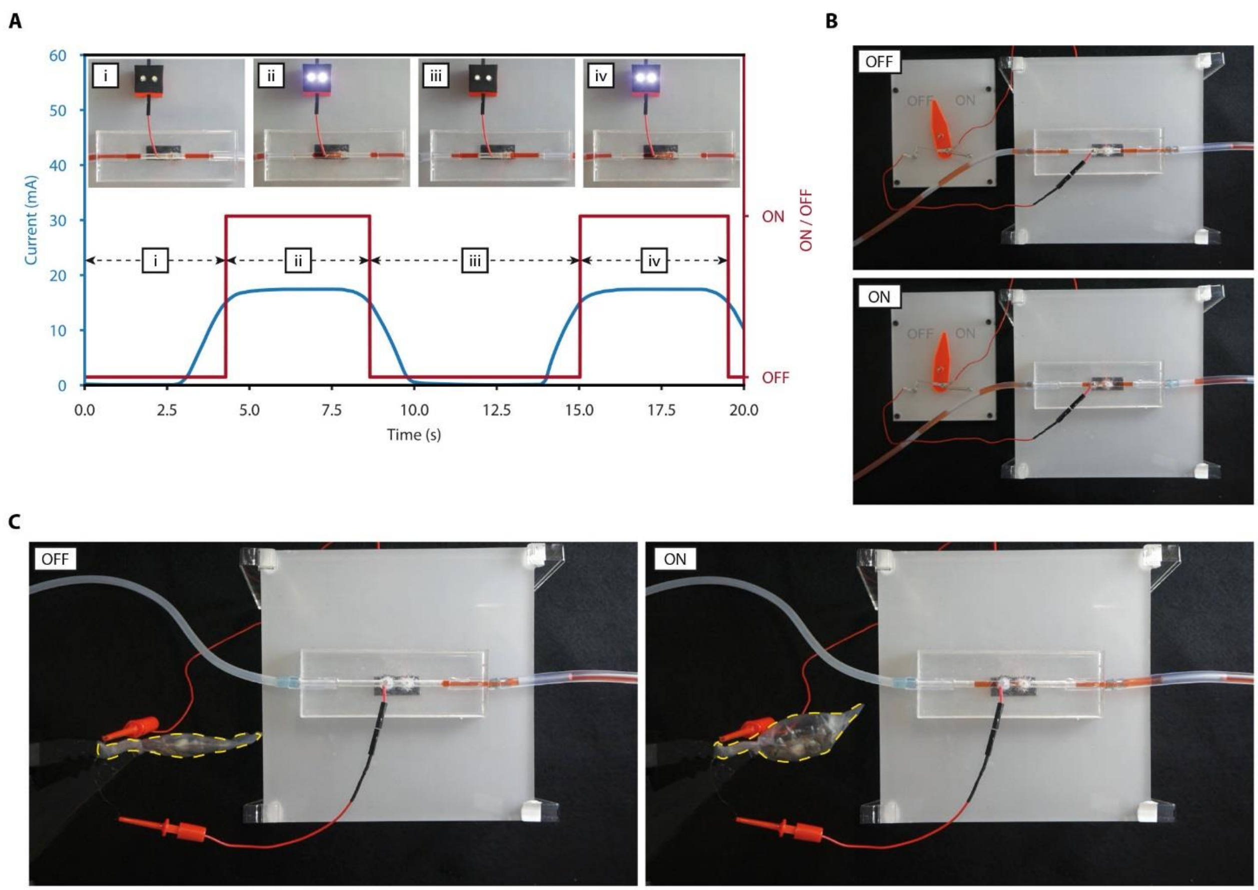

Figure S1: Three outputs controlled by Soft Matter Computers. (A) The current through two reverse polarity LEDS as they are switched by a single CFR Soft Matter computer**. (B)** An SMA driven indicator is switched by a single CFR SMC. **(C)** A pouch motor (outline indicated in yellow) is inflated via a single CFR SMC**.**

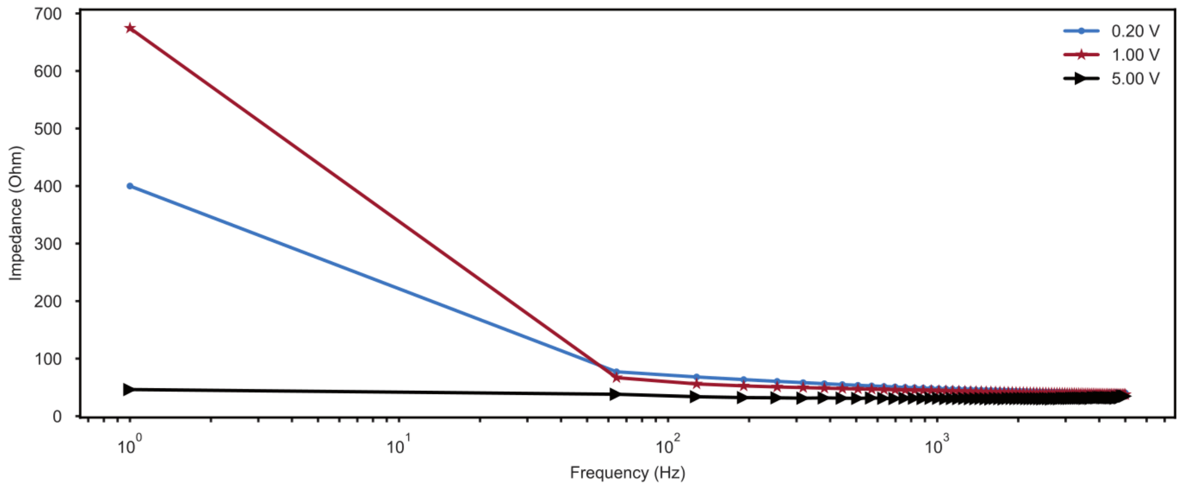

Figure S2: Frequency Response of the conductive fluid receptor at 3 voltages. In all cases, the resistance drops significantly above 100 Hz.

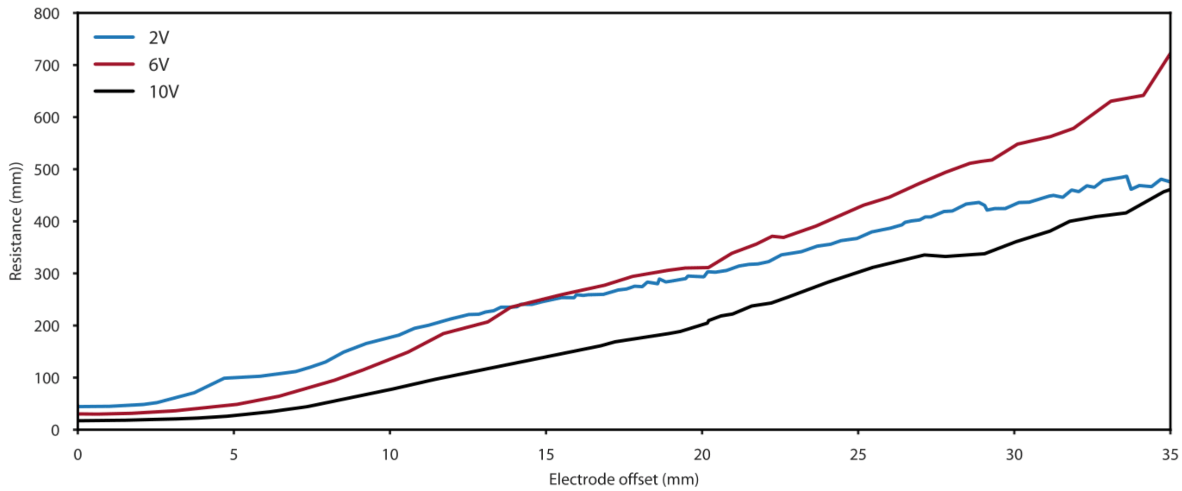

Figure S3: Resistance through a CFR as electrode offset is varied for 3 voltages. In all cases, the resistance increases linearly with offset.

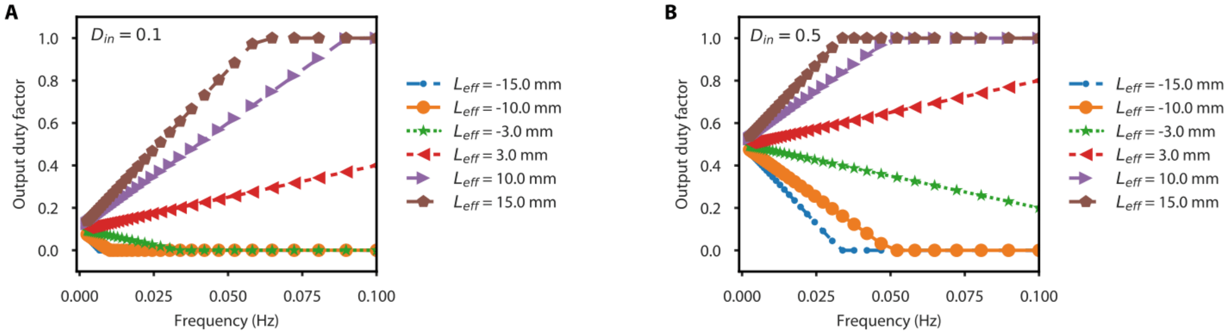

Figure S4: Frequency domain analogue computing results. (A) shows the variation in output duty factor with frequency for a fixed input duty factor of 0.1. **(B)** shows the variation in output duty factor with frequency for a fixed input duty factor of 0.5

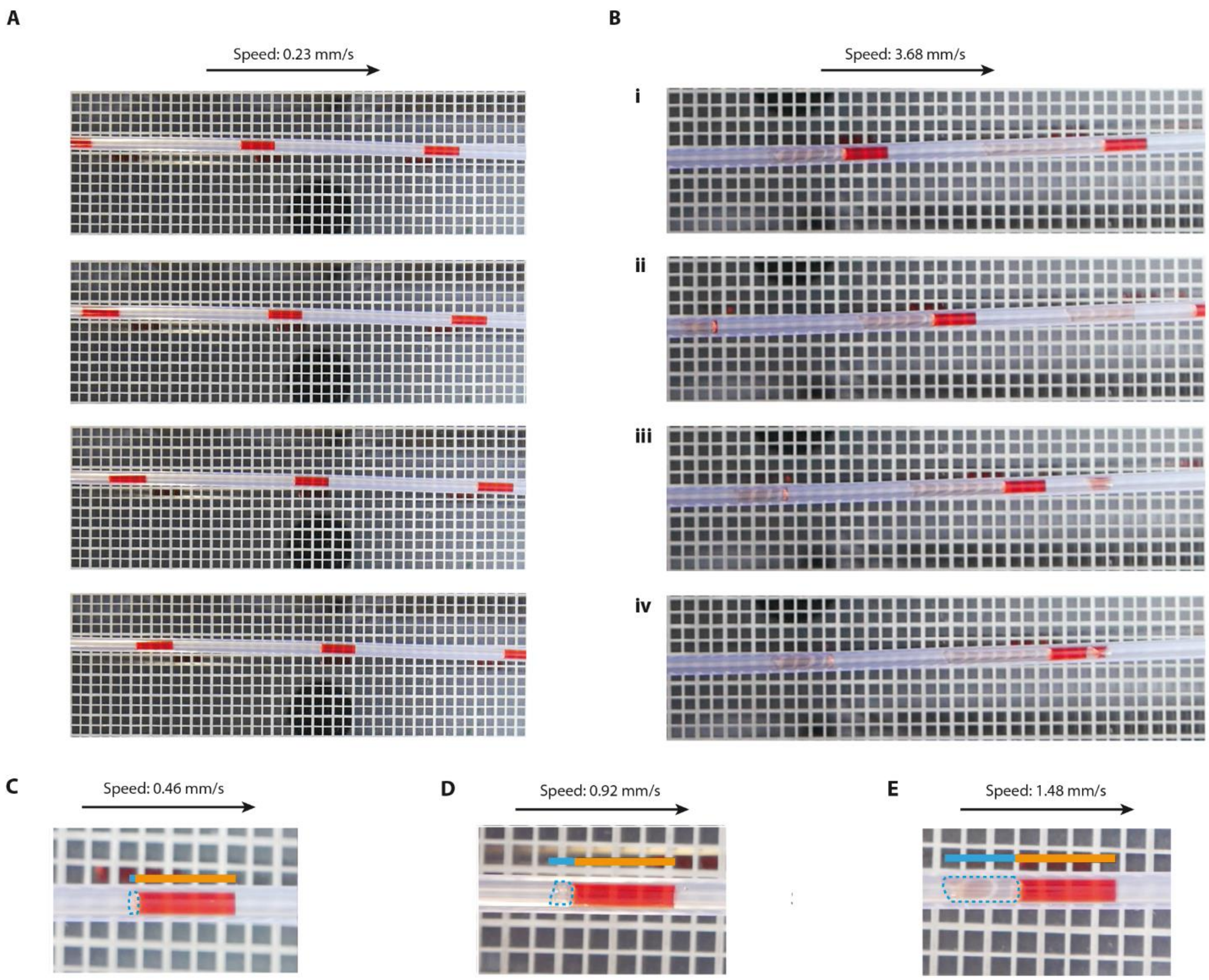

Figure S5: Stability of the fluidic tape. (A) Stable progression through the tube (speed = 0.23 mm/s) is demonstrated. **(B)** Tape breakdown at a speed of 3.68 mm/s is shown. In i), a long viscous tail has formed on the end of one conductive region. This detaches in ii), rapidly reduces in length in iii), and finally is collected by the next conductive region in iv). **(C)-(E)** The relationship between tape speed and the length of the viscous tail (blue) is shown.

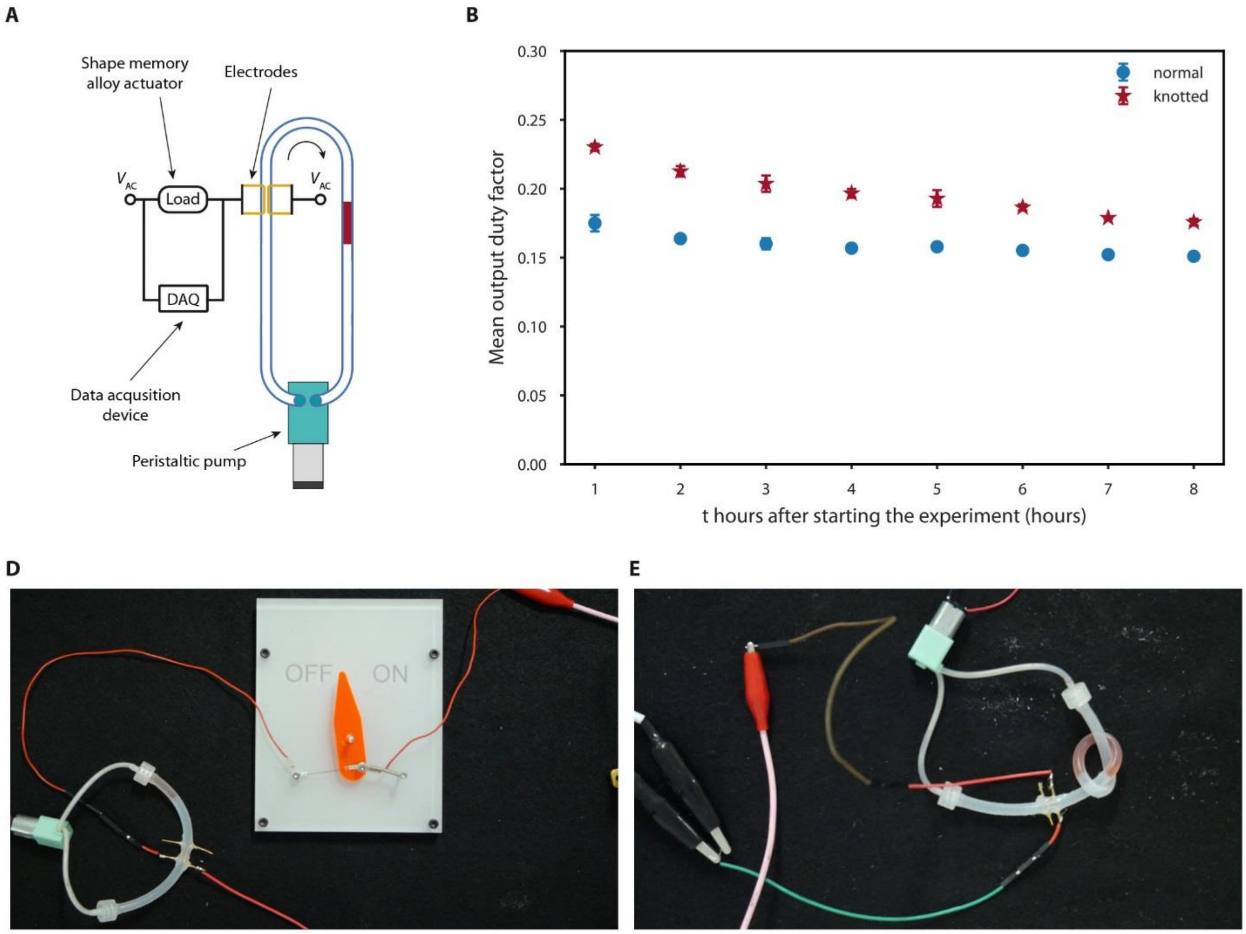

Figure S6: Long duration actuation test for undeformed and deformed tubes. (A) sketches the experimental setup, while **(B)** plots the change in mean pulse length for a normal (blue) and knotted (red) tube. **(C)** shows the normal tube, while **(D)** shows the knotted tube.

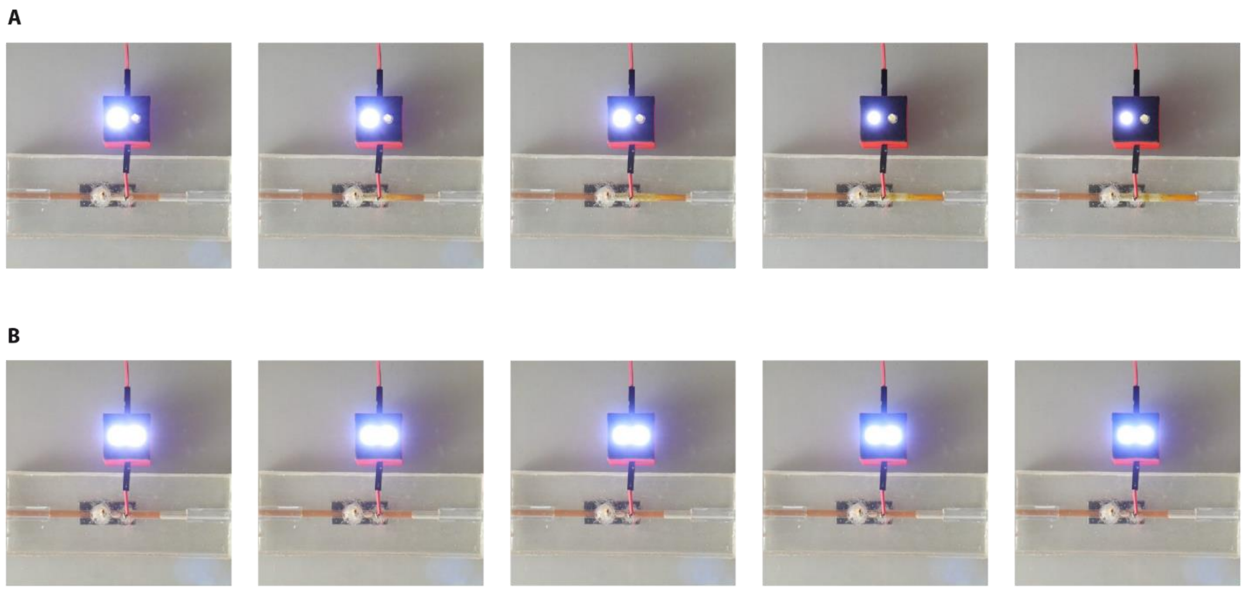

Figure S7: Electrolysis demonstration (A) shows a CFR when a DC voltage is applied. Electrolysis causes significant build up of bubbles, disrupting the CFR input pattern. **(B)** shows a CFR with a 1 kHz AC voltage is applied. No electrolysis is observed.

Movie S8: CFR Concept. A single CFR is used to drive a pair of reverse polarity LEDs. As the tape progresses through the region spanned by the electrode, the LEDs are switched.

Movie S9: CFR AND Gate. Two CFRs are electrically connected in series to an SMA driven output indicator. The mechanical inputs are pressed in sequence, and the truth table for an AND gate is generated.

Movie S10: CFR OR Gate. Two CFRs are electrically connected in parallel to an SMA driven output indicator. The mechanical inputs are pressed in sequence, and the truth table for an OR gate is generated.

Movie S11: CFR NAND Gate. Two CFRs are electrically connected in parallel to an SMA driven output indicator. The mechanical inputs are pressed in sequence, and the truth table for an NAND gate is generated.

Movie S12: CFR NOR Gate. Two CFRs are electrically connected in series to an SMA driven output indicator. The mechanical inputs are pressed in sequence, and the truth table for an NOR gate is generated.

Movie S13: Composite SMC. A CFR switch (CFR1) is connected to a CFR NOT gate (CFR2) via an Electro-fluidic diode. When the mechanical input is pressed, the switch activates the Electro-fluidic diode. The diode advances the tape inside CFR2, switching the output off.

Movie S14: SMC Softworm. Top view of the SMC Softworm. The Softworm moves forward with a *crawling* gait.

Movie S15: SMC Gripper. Top and side views of a gripper with programmed reflexes. Three inputs are pressed simultaneously, generating a *power* grip.

Movie S16: Behaviour Switching. A soft manipulator is switched between three behaviours by varying the duty factor of the input to the SMC.

Movie S17: Fast actuation demonstration. An SMC is used to control an SMA actuator at high speed.